https://doi.org/10.5194/gmd-2021-220
Preprint. Discussion started: 12 July 2021


Geoscientific Model Development Discussions
Open Access

**CAPS v1.0: An improved regional coupled modeling system for Arctic sea ice and climate simulation and prediction**

**Chao-Yuan Yang[1], Jiping Liu[2], Dake Chen[1]**

[1]School of Atmospheric Sciences, Sun Yat-sen University, and Southern Marine Science and Engineering Guangdong Laboratory (Zhuhai), Zhuhai, Guangdong, China

[2]Department of Atmospheric and Environmental Sciences, University at Albany, State University of New York, Albany, NY, USA

Corresponding author:

Chao-Yuan Yang (yangchy36@mail.sysu.eu.cn) and Jiping Liu (jliu26@albany.edu)

https://doi.org/10.5194/gmd-2021-220
Preprint. Discussion started: 12 July 2021


Geoscientific Model Development Discussions

**Abstract**

The updated Coupled Arctic Prediction System (CAPS) is evaluated, which is built on new versions of Weather Research and Forecasting model (WRF), the Regional Ocean Modeling System (ROMS), the Community Ice CodE (CICE), and a data assimilation based on the Local Error Subspace Transform Kalman Filter. A set of Pan-Arctic prediction experiments with improved/changed physical parameterizations in WRF, ROMS and CICE as well as different configurations are performed for the year 2018 to assess their impacts on the predictive skill of Arctic sea ice at seasonal timescale. The key improvements of WRF, including cumulus, boundary layer, and land surface schemes, result in improved simulation in near surface air temperature and downward radiation. The major changes of ROMS, including tracer advection and vertical mixing schemes, lead to improved evolution of the predicted total ice extent (particularly correcting the late ice recovery issue in the previous CAPS), and reduced biases in sea surface temperature. The changes of CICE, that include improved ice thermodynamics and assimilation of new sea ice thickness product, have noticeable influences on the predicted ice thickness and the timing of ice recovery. Results from the prediction experiments suggest that the updated CAPS can better predict the evolution of total ice extent compared with its predecessor, though the predictions still have certain biases at the regional scale. We further show that the CAPS can remain skillful beyond the melting season, which may have potential values for stakeholders making decisions for socioeconomical activities in the Arctic.

https://doi.org/10.5194/gmd-2021-220
Preprint. Discussion started: 12 July 2021



## 1. Introduction

Over the past few decades, the extent of Arctic sea ice has decreased rapidly and entered a thinner/younger regime associated with global climate change (e.g., Kwok, 2018; Serreze and Meier, 2019). The drastic changes in the properties of Arctic sea ice have captured attentions of a wide range of stakeholders, such as trans-Arctic shipping, natural resource exploration, and activities of coastal communities relying on sea ice (e.g., Newton et al., 2016). This leads to increasing demands on skillful Arctic sea ice prediction, particularly at seasonal timescale (e.g., Jung et al., 2016; Liu et al., 2019; Stroeve et al., 2014). However, Arctic sea ice prediction based on different approaches (e.g., statistical method and dynamical model) submitted to the Sea Ice Outlook, a community effort managed by the Sea Ice Prediction Network (SPIN, https://www.arcus.org/sipn), shows substantial biases in the predicted seasonal minimum of Arctic sea ice extent compared to the observations for most years since 2008 (Liu et al., 2019; Stroeve et al., 2014). The skills of coupled climate models (GCMs) in predicting Pan-Arctic sea ice extent have been assessed with suites of hindcasts, and these studies suggested that GCMs have skill in predicting ice extent at lead times of 1-6 months (e.g., Blanchard-Wrigglesworth et al., 2015; Chevallier et al., 2013; Guemas et al., 2016; Merryfield et al., 2013; Msadek et al., 2014; Peterson et al., 2015; Sigmond et al., 2013; Wang et al., 2013; Zampieri et al., 2018). Moreover, studies using a "perfect model" approach, which examines the skill of a model predicting itself, suggested that Arctic sea ice cover can be potentially predictable up to two years in advance (e.g., Blanchard-Wrigglesworth et al., 2011; Blanchard-Wrigglesworth and Bushuk, 2018; Day et al., 2016; Germe et al., 2014; Tietsche et al., 2014).

https://doi.org/10.5194/gmd-2021-220
Preprint. Discussion started: 12 July 2021



The gap between actual predictive skill with dynamical models and theoretical predictability suggested by "perfect model" studies may be related to inaccurate initial conditions and/or inadequate physical parameterizations in dynamical models (Stroeve et al., 2015).

Recently, we have developed an atmosphere-ocean-sea ice regional coupled modeling system, hereafter called Coupled Arctic Prediction System (CAPS), for seasonal Arctic sea ice and climate prediction (Yang et al., 2020, hereafter Y20). To improve the accuracy of initial sea ice conditions, CAPS employs an ensemble-based data assimilation system to assimilate satellite-based sea ice observations. Seasonal Pan-Arctic sea ice predictions with improved initial sea ice conditions conducted in Y20 have shown that CAPS has potential to provide skillful Arctic sea ice predictions at seasonal timescale.

With recent improvements in the model components of CAPS, this paper gives a description of the updated CAPS, and presents the assessment of seasonal Arctic sea ice predictions associated with improved/changed physical parameterizations. This paper is structured as follows. Section 2 provides an overview of the CAPS, including major changes/improvements in the model components compared to its predecessor described in Y20, as well as the data assimilation system and the assimilation procedures. Section 3 describes the designs of the prediction experiments, and examines the performance of the updated CAPS associated with major changes/improvements in the model components. Some discussions and concluding remarks and are given in section 4 and 5.

## 2. Coupled Arctic Prediction System (CAPS)

As described in Y20, to enhance our ability to predict seasonal Arctic sea ice as well as

https://doi.org/10.5194/gmd-2021-220
Preprint. Discussion started: 12 July 2021



climate, we have developed CAPS by coupling the Community Ice CodE (CICE) with the Weather Research and Forecasting Model (WRF) and the Regional Ocean Modeling System (ROMS) based on the Coupled Ocean-Atmosphere-Wave-Sediment Transport (COAWST) modeling framework (Warner et al., 2010). The advantage of CAPS is its model components have different physics options for us to choose. With community efforts on improving the WRF, ROMS, and CICE models, in this study, we update CAPS based on newly-released WRF, ROMS, and CICE models for further development of our Arctic sea ice prediction system. Table 1 provides the versions for these model components between this paper and Y20. The same physical parameterizations described in Y20 are used here for the control simulation, but some of them are improved as the WRF, ROMS, and CICE models released their new versions (see Table 2). Major changes in physics parameterization and the model infrastructure in the WRF, ROMS, and CICE models are described below.

### 2.1. Model components and updates

WRF: The WRF model (Skamarock et al., 2005) is a non-hydrostatic and quasi-compressible model, which uses hybrid vertical coordinate with the top of the model at 50 mb and the Arakawa C-grid in horizontal. The Rapid Refresh (RAP) system, a high-frequency, continental-scale weather prediction/assimilation modeling system operational at the National Centers for Environmental Prediction (NCEP), has made some improvements in the WRF model physics (Benjamin et al., 2016). The official release of WRF model since version 3.9 has adapted these modified physics parameterizations in the RAP system, including the Grell-Freitas convection scheme (GF) and the Mellor-Yamada-Nakanishi-Niino planetary boundary

https://doi.org/10.5194/gmd-2021-220
Preprint. Discussion started: 12 July 2021



layer (PBL) scheme (MYNN) as the replacement of original schemes in the WRF model. For the GF scheme, the major improvements compared to the original scheme (Grell and Freitas, 2014) include: 1) a beta probability density function used as the normalized mass flux profile for representing height-dependent entrainment/detrainment rates within statistical-averaged deep convective plumes, and 2) the European Centre for Medium-Range Weather Forecasts (ECMWF) approach used for momentum transport due to convection (Biswas et al. 2020; Freitas et al. 2018). For the MYNN scheme, compared to the original scheme (Nakanishi and Nino, 2009), the RAP system improved the mixing-length formulation and removed numerical deficiencies to better represent subgrid-scale cloudiness (Benjamin et al. 2016, see Append. B).

For the Noah land surface model (Chen and Dudhia, 2001), some issues including discontinuous behavior for soil ice melting and negative moisture fluxes over glacial and sea ice, as well as minor issues associated with snow melting have been fixed since the release of WRF version 3.9.

ROMS: The ROMS model is a terrain-following and free-surface model, which solves three-dimensional Reynolds-averaged Navier-Stokes equations with the hydrostatic and Boussinesq approximation (Shchepetkin and McWilliams, 2005; Haidvogel et al., 2008). In the vertical, the equations are discretized over bottom topography with stretching terrain-following coordinates (Song and Haidvodel, 1994). In the horizontal, the ROMS model uses boundary-fitted, orthogonal curvilinear coordinates on a staggered Arakawa C-grid. In the updated CAPS, the major change in the latest ROMS model is associated with surface heat/freshwater fluxes and their coupling to other model components. This change prevents the potentially erroneous

https://doi.org/10.5194/gmd-2021-220
Preprint. Discussion started: 12 July 2021

Geoscientific Model Development Discussions

results when the ROMS timestep is smaller than the coupling frequency with other model components. Other changes in the ROMS model of the updated CAPS can be found in the ROMS distribution website (https://www.myroms.org/projects/src/report/4 Ticket #654 to #824).

CICE: The CICE model is designed to be a sea ice model component for global coupled climate models. Its dynamic core simulates the movement of sea ice based on forces from the atmosphere, the ocean, and Earth's rotation and the material strength of the ice. The new feature of CICE version 6.0.0 contains an independent software package, Icepack, to provide the column physics code for all thermodynamic parameterizations in a single grid-cell. These parameterizations include the MUSHY-layer ice thermodynamics (Turner et al., 2013) that resolves prognostic vertical temperature and salinity profiles. The new version of CICE also includes improvements in sea ice rheology and a new landfast-ice parameterization (Lemieux et al., 2016). More details can be found in the CICE Consortium GitHub page (https://github.com/CICE-Consortium).

### 2.2. Data Assimilation and evaluation data

As described in Y20, the Parallel Data Assimilation Framework (PDAF, Nerger and Hiller, 2013) was implemented in CAPS for assimilating sea ice observations, which provides a variety of optimized ensemble-based Kalman filters including the Local Ensemble Transform Kalman Filter (LETKF; Hunt et al., 2007), the Localized Singular Evolutive Interpolated Kalman (LSEIK; Nerger et al., 2006), and the Local Error Subspace Transform Kalman Filter (LESTKF; Nerger et al., 2012). Following Y20, the LESTKF is used to assimilate satellite-

https://doi.org/10.5194/gmd-2021-220
Preprint. Discussion started: 12 July 2021



observed sea ice parameters. The LESTKF projects the ensemble onto the error subspace and then directly computes the ensemble transformation in the error subspace. This results in better assimilation performance compared to the LSEIK filter and higher computational efficiency compared to the LETKF as discussed in Nerger et al. (2012).

The initial ensembles are generated by applying the second-order exact sampling (Pham, 2001) to sea ice state vectors (ice concentration and thickness) from an one-month free run, and assimilating sea ice observations that include: 1) the near real-time daily Arctic sea ice concentration processed by the National Aeronautics and Space Administration (NASA) Team algorithm (Maslanik and Stroeve, 1999) obtained from the National Snow and Ice Data Center (NSIDC; https://nsidc.org/data/NSIDC-0081/), 2) a combined monthly sea ice thickness derived from the CryoSat-2 (Laxon et al., 2013; obtained from http://data.seaiceportal.de), and daily sea ice thickness derived from the Soil Moisture and Ocean Salinity (SMOS; Kaleschke et al., 2012; Tian-Kunze et al., 2014; obtained from https://icdc.cen.uni-hamburg.de/en/l3c-smos-sit.html). To address the issue that sea ice thickness derived from CyroSat-2 and SMOS are unavailable during the melting season, the melting season ice thickness is estimated based on the seasonal cycle of the Pan-Arctic Ice Ocean Modeling and Assimilation System (PIOMAS) daily sea ice thickness (Zhang and Rothrock, 2003) as described in Y20.

In this study, compared with Y20, we change the localization radius from 2 to 6 grids during the assimilation procedures. The sea ice component in the updated CAPS experienced some instability at initial simulations with 2 localization radii but not with 6 localization radii. Figure 1 shows that initial sea ice thickness after the data assimilation with (a) 2 localization radii and 1.5 m uncertainty for assimilating ice thickness and (b) 6 localization radii and 0.75 m uncertainty. The initial ice thickness for both configurations has similar spatial distribution. However, the ice thickness with 2 localization radii and 1.5 m uncertainty shows discontinuous features (Fig. 1a), which results in numerical instability during the initial model integration. Such discontinuous feature is obviously corrected with 6 localization radii and 0.75 m uncertainty (Fig. 1b). Following Y20, here we test the 2018 prediction experiment with 2 and 6 localization radii but the same uncertainty for ice thickness (0.75m) for the data assimilation (Y20 and Y20_MOD, see Table 3). The Y20 and Y20_MOD experiments show very similar temporal evolutions of the total sea ice extent, although Y20_MOD (red solid line) predicts slightly less ice extent than that of Y20 (blue line) for the July experiment (Figure 2). In this study, the configuration of Y20_MOD is designated as the reference for the following assessment of the updated CAPS.

For the evaluation of sea ice prediction, Sea Ice Index (Fetterer et al., 2017; obtained from https://nsidc.org/data/G02135) is used as the observed total sea ice extent, and the NSIDC sea ice concentrations derived from Special Sensor Microwave Imager/Sounder (SSMIS) with the NASA Team algorithm (Cavalieri et al., 1996; obtained from https://nsidc.org/data/nsidc-0051) is employed. For the assessment of the atmospheric and oceanic variables, the ECMWF reanalysis version 5 (ERA5; Hersbach et al., 2020; obtained from https://cds.climate.copernicus.eu) and National Oceanic and Atmospheric Administration (NOAA) Optimum Interpolation (OI) Sea Surface Temperature (SST) (Reynolds et al., 2007; obtained from https://psl.noaa.gov/data/gridded/data.noaa.oisst.v2.highres.html) are utilized.

https://doi.org/10.5194/gmd-2021-220
Preprint. Discussion started: 12 July 2021

Geoscientific Model Development Discussions
Open Access
EGU

## 3. Model Evaluation

### 3.1. Experiment designs

Following Y20, the model domain includes 319 (449) x- (y-) grid points with a ~24 km grid spacing for all model components (see Figure 2 in Y20). The WRF model uses 50 vertical levels, the ROMS model uses 40 vertical levels, and the CICE model uses 7 ice layers, 1 snow layer, and 5 categories of sea ice thickness. The coupling frequency across all model components is 30 minutes. Initial and boundary conditions for the WRF and ROMS models are generated from the Climate Forecast System version 2 (CFSv2, Saha et al., 2014) operational forecast archived at NCEP (http://nomads.ncep.noaa.gov/pub/data/nccf/com/cfs/prod/). Sea ice initial conditions are generated from the data assimilation described in section 2.2. Ensemble predictions with 8 members are conducted. A set of numerical experiments for the Pan-Arctic seasonal sea ice prediction with different configurations, starting from July 1st to October 1st for the year of 2018, has been conducted. Table 3 provides the details of these experiments that allow us to examine impacts of improved/changed physical parameterizations in the updated CAPS on sea ice prediction at seasonal timescale.

### 3.2. Impacts of the RAP physics in the WRF model

To examine the performance the updated CAPS compared to its predecessor in Y20, the Y21_CTRL experiment uses some updated physics configurations in the WRF model as listed in Table 2. The temporal evolution of the ensemble mean of the predicted Arctic sea ice extent for the Y21_CTRL and Y20_MOD experiments along with the NSIDC observations are shown in Figure 3. The ice extent is calculated as the sum of area of all grid cells with ice concentration

https://doi.org/10.5194/gmd-2021-220
Preprint. Discussion started: 12 July 2021



greater than 15%. Besides the total ice extent, we also calculate ice extent for the following subregions: 1) Beaufort and Chukchi Seas (120W-180, 60N-80N), 2) East Siberian and Laptev Seas (90E-180, 60N-80N), 3) Barents, Kara, and Greenland Seas (30W-90E, 60N-80N), 4) Canadian Archipelago and Baffin Bay (30W-120W, 60N-80N). To further assess the predictive skill of our predictions, here we also show the climatology prediction (CLIM, the period of 1998-2017) and the damped anomaly persistence prediction (DAMP). Following Van den Dool (2006), the DAMP is generated from the initial sea ice extent anomaly (relative to the 1998-2017 climatology) scaled by the autocorrelation and the ratio of standard deviation between different lead times and initial times (see the DAMP equation in Y20).

Compared to the Y20_MOD experiment, the Y21_CTRL experiment has ~0.5 million km$^2$ more ice extent at the initial, but the ice in Y21_CTRL melts faster than Y20_MOD during the first 2-week integration. After that, they track each other closely, and predict nearly the same minimum ice extent (~4.3 million km$^2$). Like Y20_MOD, Y21 still has a delayed ice recovery in late September. Compared with the CLIM/DAMP predictions (black dashed and dotted lines), both Y20_MOD and Y21_CTRL have smaller biases after early August. At the regional scale, in the Beaufort-Chukchi Seas, Y21_CTRL predicts slower ice retreat after late July than that of Y20_MOD, whereas in the East Siberian-Laptev Seas, Y20_MOD shows slower ice decline after mid-July than that of Y21_CTRL (Fig. 3a, 3b). Both Y20_MOD and Y21_CTRL agree well with the observations in the Barents-Kara-Greenland Seas (Fig. 3c). In the Baffin Bay-Canadian Archipelago, both Y20_MOD and Y21_CTRL have similar temporal evolution but show systematic underestimation of the observed areal extent (~0.3 million km$^2$, Fig. 3d).

This underestimation is partly due to the difference in land/sea mask (particularly in the Canadian Archipelago) between our model grid and the NSIDC grid (not shown).

Figure 4 shows the spatial distribution of the NSIDC sea ice concentration and the difference between the predicted sea ice concentration and the observations for all grid cells that the predictions and the observations both have at least 15% ice concentration for the Y20_MOD and Y21_CTRL experiments. The vertical and horizontal lining areas represent difference of the ice edge location. The distribution of the predicted ice concentration anomalies resembles in both Y20_MOD and Y21_CTRL experiments, except Y21_CTRL predicts relatively higher ice concentration in much of the Beaufort, Chukchi, and East Siberian Seas for the entire period (Fig. 4d-i).

In a fully coupled predictive model, sea ice is determined by the fluxes from the atmosphere above and the ocean below. The major difference between Y20_MOD and Y21_CTRL is the RAP physics improvements in the WRF model. The RAP physics improvements can have profound influence on the behavior of simulated atmospheric variables (i.e., radiation, temperature, humidity, precipitation, and wind). Figure 5 shows the spatial distribution of the ERA5 2m air temperature (T2), the predicted anomalies (ensemble mean minuses ERA5) of Y20_MOD, and the difference between Y21_CTRL and Y20_MOD. For Y20_MOD, the predicted air temperature in July has small cold (warm) biases over all ocean basins (northern Greenland and eastern coastal Siberia), small-to-moderate cold biases (~3-5 degrees) over Canada and Siberia, and moderate-to-large cold biases (~6-9 degrees) over eastern Europe (Fig. 5d). In August (Fig. 5e), the cold biases over most of the model domain

https://doi.org/10.5194/gmd-2021-220
Preprint. Discussion started: 12 July 2021



are increased. In particular, very large cold bias (over 10 degrees) are located over east Siberia. In September, these cold biases are decreased, and warm biases are found in the north of Greenland and Canada (Fig. 5f). With the adaptation of the RAP physics in the updated WRF model, Y21_CTRL, in general, produces a warmer state in most of the model domain compared to that of Y20_MOD during the entire prediction period. For July (Fig. 5g), the predicted air temperature is slightly warmer (< 1 degrees) over the Arctic Ocean, the Pacific, and Atlantic sectors, moderately warmer (~1-2 degrees) over the Siberia coast and Canadian Archipelago, but the slightly colder (<1 degrees) over northeastern Europe and northern Canada than that of Y20_MOD. For August (Fig. 5h), the Arctic Ocean and Atlantic sector (the Pacific sector and northern Canada) are relatively warmer (colder) than that of Y20_MOD. Excessive cold biases shown in Y20_MOD over Siberia are reduced notably (~2.5-4 degrees) in Y21_CTRL. As discussed above, Y21_CTRL has faster ice melting in the East Siberian-Laptev Seas, which can be partly attributed to the changes in the predicted air temperature.

Figure 6 and Figure 7 shows the spatial distribution of the ERA5 downward solar and thermal radiation at the surface (SWDN and LWDN), the predicted anomalies (ensemble mean minuses ERA5) of Y20_MOD, and the difference between Y20_MOD and Y21_CTRL. For July, Y20_MOD (Fig. 6d) results in less SWDN over most of ocean basins, southern Canada, western Siberia, and eastern Europe while more SWDN over southern and eastern Siberia, Canadian Archipelago, and northern Canada compared with ERA5. For August and September (Fig. 6e-f), the spatial distribution, in general, is similar to that of July, except that eastern Siberia, Canadian Archipelago and northern Canada have opposite sign. It also shows that the

https://doi.org/10.5194/gmd-2021-220
Preprint. Discussion started: 12 July 2021

Geoscientific Model Development Discussions
Open Access
EGU

magnitude of biases decreases as the lead time decreases. With the RAP physics in the Y21_CTRL experiment, large areas have smaller biases compared with Y20_MOD in July (i.e., the positive difference between Y21_CTRL and Y20_MOD corresponds to the negative biases in Y20_MOD), except the north Pacific (especially the Sea of Okhotsk), southern Canada, and the central coastal Siberia (Fig. 6g). For August (Fig. 6h), there are more areas with smaller biases, but the north Pacific and southern Canada still have larger biases. In contrast to SWDN, the biases of LWDN shown in Y20_MOD has smaller magnitude (up to 100 W/m2 in SWDN vs. 50 W/m2 in LWDN) for the entire prediction period (Fig. 7d-f). For July, Y20_MOD (Fig. 7d) shows less LDWN over most of the model domain compared with ERA5, except the Atlantic sector and north of Greenland. For August, areas with negative biases expand and the magnitude of biases increases (particularly in eastern and southern Siberia) compared with that of July (Fig. 7e). For September (Fig. 7f), the spatial distribution of LWDN is mostly similar to that of July, except that northern Canada and Canadian Archipelago show positive biases. The Y21_CTRL experiment with the RAP physics tends to reduce the negative biases shown in Y20_MOD, especially the negative biases over Siberia in August and September (Fig. 7g-i).

Associated with the change in surface fluxes, compared to Y20_MOD, Y21_CTRL shows warmer SST along the ice edge in July, and the warm difference along the ice edge becomes larger (particularly near the east Siberian coast) in August and September. The other areas in Y21_CTRL are mostly with less than 0.2 degrees difference relative to Y20_MOD (Fig. 10g-i).

### 3.3. ROMS configuration

As described in section 2, the ROMS model uses a generalized topography-following coordinate, but currently has two vertical coordinate transformations:

$$z(x,y,\sigma,t) = S(x,y,\sigma) + \zeta(x,y,t)\left[1 + \frac{S(x,y,\sigma)}{h(x,y)}\right] \quad (1)$$
$$S(x,y,\sigma) = h_c\sigma + [h(x,y) - h_c]C(\sigma)$$

or

$$z(x,y,\sigma,t) = \zeta(x,y,t) + [\zeta(x,y,t) + h(x,y)]S(x,y,\sigma)$$
$$S(x,y,\sigma) = \frac{h_c\sigma + h(x,y)C(\sigma)}{h_c + h(x,y)} \quad (2)$$

where $S(x,y,\sigma)$ is a nonlinear vertical transformation function, $\zeta(x,y,t)$ is the free-surface, $h(x,y)$ is the unperturbed water column thickness, $C(\sigma)$ is the non-dimensional, monotonic, vertical stretching function, and $h_c$ controls the behavior of the vertical stretching. In Y20, we used the transformation (1) and the vertical stretching function introduced by Song and Haidvogel (1994) as the setup for seasonal Arctic sea ice prediction. However, the vertical transformation (1) has an inherent limitation for the value of $h_c$ (expected to be the thermocline depth), which must be less than or equal to the minimum value in $h(x,y)$. As the result, $h_c$ was chosen as 10 meters due to the limitation of the minimum value in $h(x,y)$ in Y20. This limitation is removed with the vertical transformation (2) and $h_c$ can be any positive value. Currently, the vertical transformation (2) and the vertical stretching function introduced by Shchepetkin (2010, the function in a research version of ROMS developed at University of California, Los Angeles, https://www.myroms.org/wiki/Vertical_S-coordinate) are employed. The Y21_VT experiment is designed to examine the impacts of the vertical transformation in the ROMS model on seasonal sea ice prediction by using the vertical transformation (2), the Shchepetkin stretching function, and 300 meters for $h_c$.

In pervious sensitivity experiments to determine the choice of ROMS physical parametrizations listed in Table 2, we noticed that the tracer advection and the vertical mixing schemes have important effects on sea ice simulation. Thus here the Y21_RP experiment is designated to further explore the influence of these schemes in the updated CAPS, in which the tracer advection scheme is changed from Multidimensional positive definite advection transport algorithm (MPDATA; Smolarkiewicz, 2006) to the third-order upwind horizontal advection (U3H; Rasch, 1994; Shchepetkin, and McWilliams, 2005) and the fourth-order centered vertical advection schemes (C4V; Shchepetkin, and McWilliams, 1998; 2005).

The temporal evolutions of the ensemble mean of the predicted Arctic total sea ice extent (as well as regional ice extent) for Y21_CTRL, Y21_VT, and Y21_RP are shown in Figure 8. Y21_VT (green line) simulates slightly less areal extent (<0.1 million km$^2$) compared to that of Y21_CTRL throughout the prediction period. The Y21_RP shows highly similar temporal evolution of areal extent as Y21_CTRL until near the end of August. After that, the ice melting slows down and ice extent begins to recover earlier in Y21_RP (red line) compared to both Y21_CRTL and Y21_VT, which leads to much smaller biases in seasonal minimum ice extent relative to the observation. This result suggests the delayed ice recovery in late September shown in Y20, Y20_MOD and Y21_CTRL is partly due to the choice of ocean advection and vertical mixing schemes that change the behavior of oceanic state. Y21_RP also shows much better predictive skill after late August compared with the CLIM/DAMP predictions (black dashed and dotted lines). At the regional scale, changes in both the ocean vertical coordinate (Y21_VT) and the advection and vertical mixing scheme (Y21_RP) do not significantly affect

https://doi.org/10.5194/gmd-2021-220
Preprint. Discussion started: 12 July 2021



the evolution of areal extent in the Barents-Kara-Greenland Seas and the Baffin Bay-Canadian Archipelago compared to that of Y21_CTRL (Fig. 8c, d). However, Y21_VT agrees better with the observations in the Beaufort-Chukchi Seas and the East Siberian-Laptev Seas compared to that of Y21_CTRL and the ice extent of Y21_RP stops retreating after mid-September in the Beaufort-Chukchi Seas relative to that of Y21_CTRL (Fig. 8a, b).

Spatially, the choice of vertical transformation in Y21_VT does not significantly change the distribution of sea ice biases in Y21_CTRL (i.e., higher ice concentration in the Pacific sector, and lower ice concentration in the Atlantic sector, (Fig. 9a-c, Fig. 4g-i). The Y21_VT experiment has slightly lower ice concentration compared with that of Y21_CTRL, which corresponds to less areal extent of Y21_VT shown in Figure 8. By using U3H/C4V advection scheme, the Y21_RP experiment has positive anomalies for most ice-covered areas (Fig. 9d-f). For September, the Y21_RP experiment better predicts the ice edge location in the Atlantic sector of the Arctic Ocean (i.e., smaller areas with horizontal/vertical lining) compared to the experiments described above (Fig. 9f).

Figure 10 shows that spatial distribution of the SST changes of Y21_VT and Y21_RP relative to Y21_CTRL (as well as predicted anomalies of Y20_MOD and the difference between Y21_CTRL and Y21_MOD). By using different vertical transformation in the ROMS model, the Y21_VT experiment simulates slightly warmer SST in the north Pacific and Atlantic (~0.5 degree), and colder SST in the Bering Sea, Sea of Okhotsk, Barents-Kara, and Greenland Seas (~0.5-1.0 degree). We also note that SST under sea ice cover is warmer than that of Y21_CTRL, especially in the Beaufort-Chukchi Seas, which results in larger temperature difference and thus heat fluxes at the ice-ocean interface, and then contributes to faster ice retreating in the Beaufort-Chukchi Seas (Fig. 10j-l, Fig. 8a). With U3H/C4V tracer advection scheme in Y21_RP, cold biases shown in Y21_CTRL (Fig. 10d-i) are reduced significantly in the north Pacific and Atlantic, but SST under ice cover is slightly colder than that of Y21_CTRL (Fig. 10m-o).

**3.4. CICE configuration and ice thickness assimilation**

In Y20, we used the ice thermodynamics introduced by Bitz and Lipscomb (1999; hereafter BL99), which assumes a fixed vertical salinity profile based on observations, as the setup for seasonal Arctic sea ice prediction. Since the release of CICE version 5, it includes the MUSHY-layer ice thermodynamics introduced by Turner et al. (2013), which simulates vertically resolved and time-varying prognostic salinity and its associated impact on other thermodynamics properties of sea ice. In the Y21_MUSHY experiment, we change ice thermodynamics from BL99 to MUSHY (Table 3) to examine whether improved ice thermodynamics has noticeable influence on sea ice prediction at seasonal timescale. Additionally, in Y20 and prediction experiments discussed above, we use a simple approach to merge CryoSat-2 and SMOS ice thickness by replacing ice thickness less than 1m in CryoSat-2 data with SMOS data for ice thickness assimilation. Ricker et al. (2017) presented a new ice thickness product (CS2SMOS) based on the optimal interpolation to statistically merge CrySat-2 and SMOS data. The Y21_SIT experiment (Table 3) is designed to investigate the impacts of assimilating different approaches to merge CyroSat-2 and SMOS data on sea ice prediction .

Figure 11 shows the temporal evolutions of the ensemble mean of the predicted Arctic

https://doi.org/10.5194/gmd-2021-220
Preprint. Discussion started: 12 July 2021


Geoscientific Model Development Discussions
Open Access

total sea ice extent (as well as regional ice extent) for the Y21_RP, Y21_MUSHY, and Y21_SIT experiments. All three experiments predict almost identical total ice extents during the first 2-week integration. After that, Y21_MUSHY (red solid line) produces a slightly more ice extent (~0.2 million km$^2$) than that of Y21_RP (blue solid line) for the rest of integration, which mainly due to an increase of sea ice in the East Siberian-Laptev Seas (Fig. 11b). The timing of minimum ice extent occurs early in Y21_MUSHY relative to Y21_RP, resulting in early recovery. In contrast to Y21_RP, Y21_SIT (green solid line) simulates slightly larger ice extent after the first week of August. At the regional scale, compared with Y21_RP, Y21_SIT predicts more ice before the mid-August and less ice after that in the Beaufort-Chukchi Seas (Fig. 11a) and larger ice extent throughout the entire prediction period in the Barents-Kara-Greenland Seas (Fig. 11c). For the spatial distribution of ice concentration anomalies, Y21_MUSHY and Y21_SIT show similar distribution as Y21_RP with slightly higher ice concentration at gridpoint scale (not shown).

Figure 12 show the ensemble mean of predicted sea ice thickness of the Y21_RP, Y21_MUSHY, and Y21_SIT experiments and the ice thickness changes of Y21_MUSHY and Y21_SIT relative to Y21_RP. All three experiments produce similar ice thickness distribution, that is the thickest ice locates near the Canadian Archipelago and the Lincoln Sea, as well as the thickness gradient directs toward the Siberia coast (Fig. 12a-f). Compared with Y21_RP, Y21_MUSHY simulates thicker ice (from ~0.14m in July to over 0.2m in September) in the Canadian Arctic and the central Arctic Ocean, thinner ice (over 0.2m) in the Kara Sea in September, and negligible thickness difference in other areas (Fig. 12$g_1$-$i_1$). This is consistent with previous studies showing that the Mushy-layer thermodynamics simulates thicker ice than BL99 thermodynamics in both standalone CICE (Turner and Hunke, 2015) and the fully-coupled context (Bailey et al., 2020). Compared with Y21_RP, Y21_SIT predicts thicker ice most of the ice edge zone and thinner ice in the central Arctic Ocean in July and August. In September, Y21_SIT simulates much thinner ice (over 0.2m) in the Beaufort, Chukchi, East Siberian Seas, and the central Arctic Ocean along with thicker ice in the Barents, Kara, and Laptev Seas (Fig. 12$g_2$-$i_2$). The evolution of predicted ice thickness in Y21_SIT corresponds to that of regional ice extent shown in Figure 11. This result suggests that assimilating the new ice thickness product (CS2SMOS) have significant influences on the predicted ice thickness at the regional scale.

## 4. Discussions

Arctic sea ice prediction experiments conducted in this study follow the protocol of Sea Ice Prediction Network (SPIN), in which the outlook start from June $1^{st}$, July $1^{st}$, and August $1^{st}$ to predict seasonal minimum of ice extent in September. Due to the socioeconomic impacts of sea ice recovery during the freeze-up period (e.g., trans-Arctic shipping, coastal activities), it is also essential to investigate the predictive capability of CAPS beyond the SPIN prediction period. Combining the entire prediction period provided by CFS forecasts and the Y21_SIT experiment, the Y21_EXT-7 experiment is designed to extend the prediction period to the end of January next year (Table 3). Figure 13 shows the temporal evolutions of the ensemble mean of the predicted Arctic total sea ice extent (as well as regional ice extent) for the Y21_EXT-7 experiment. As shown in Figure 13, the predicted total ice extent exhibits reasonable evolution in terms of seasonal minimum and timing of recovery compared with the observations until late November. Y21_EXT-7 also performs better than that of the CLIM/DAMP predictions (black dashed and dotted lines) until mid-to-late November. After that, Y21_EXT-7 overestimates the total ice extent compared with the observations, and this overestimation is largely contributed by more extensive sea ice in the Barents-Kara-Greenland Seas (Fig. 13c). The overestimated ice cover in the Barents-Kara-Greenland Seas may be the results of biases from the CFS data propagated into the model domain through lateral boundary conditions and accumulated effects of biases in model components.

A growing number of studies have shown evidences of Arctic sea ice spring predictability barrier, which is defined as a springtime date that predictions initialized prior to this date have much lower predictive skill than predictions initialized after/on that date (e.g., Bonan et al., 2019; Bushuk et al., 2017; 2018; Day et al., 2014). To investigate the predictive capability of CAPS initialized prior to the summer melting season, the Y21_MAR-7 experiment is initialized on March 1$^{st}$, 2018 and predicts sea ice evolution until the end of September (Table 3). Figure 14 shows the temporal evolutions of the ensemble mean of the predicted Arctic total sea ice extent (as well as regional ice extent) for the Y21_MAR-7 experiment. The evolution of predicted total sea ice extent shows faster ice melting rate than the observations after mid-May, slower ice retreating after mid-July, and the predicted minimum of ice extent has an overestimation (~1.2 million km$^2$) compared to the observed minimum. In contrast to Y21_MAR-7, the DAMP prediction (black dotted line) agrees better with the observations throughout the 7-month prediction period. At the regional scale, Y21_MAR-7 shows abrupt ice

https://doi.org/10.5194/gmd-2021-220
Preprint. Discussion started: 12 July 2021

Geoscientific Model Development Discussions

decline after May in the Beaufort-Chukchi Seas (Fig. 14a), and this decline is mainly contributed by ice melting along the Alaskan coast (not shown). Sea ice in the East Siberian-Laptev Seas exhibits slow melting after July (Fig. 14b), and ice cover areas still connect to the Siberian coast, which is different from the observations (not shown). For the Barents-Kara-Greenland Seas (Baffin Bay-Canadian Archipelago), there are systematic overestimations (underestimations) throughout the entire prediction period (Fig. 14c-d). Bushuk et al. (2020) suggested that Arctic sea ice predictability prior to the barrier date is mainly limited by synoptic events, which are only predictable for few weeks, whereas the predictability after the barrier date is enhanced by ice-albedo feedback with the onset of ice melting.

## 5. Conclusions

This paper presents and evaluates the updated Coupled Arctic Prediction System (CAPS) designated for Arctic sea ice and climate prediction. The CAPS consists of the WRF, ROMS, and CICE models under the framework of the COAWST system, as well as data assimilation system based on the localized error subspace transform ensemble Kalman filter to assimilate satellite-observed sea ice observations. A set of Pan-Arctic prediction experiments with improved/changed physical parameterizations as well as different configurations starting from July 1st to the end of September are performed for the year of 2018 to assess their impacts of the updated CAPS on the predictive skill of sea ice at seasonal timescale.

The results of prediction experiments show that the updated CAPS with improved physical parameterizations can better predict the evolution of the total ice extent compared with its predecessor described in Yang et al. (2020), though the predictions exhibit biases in regional

https://doi.org/10.5194/gmd-2021-220
Preprint. Discussion started: 12 July 2021



ice extent. We demonstrate that the CAPS can remain skillful beyond the designated period of Sea Ice Prediction Network (SIPN), which has potential values for stakeholders making decisions regarding the socioeconomical activities. Along with the improved predictive skill of total sea ice extent, the updated CAPS also has reduced biases in the predicted near surface air temperature, downward radiations at the surface, and sea surface temperature in Arctic domain compared to its predecessor. Based on the prediction experiments discussed in the paper, the configuration of the Y21_SIT experiment is assigned as the finalized CAPS version 1.0. Improving the representation of physical processes in the CAPS version 1.0 for further reducing the model bias will remain the main focus for the development of CAPS version 1.0.

Since the CAPS version 1.0 is a regional modeling system, it relies on GCM forecasts as initial and lateral boundary conditions. That is, biases existed in GCM simulations (here the CFS forecast) can be propagated into and affect the entire area-limited domain (e.g., Bruyère et al., 2014; Rocheta et al., 2020; Wu et al., 2005). This issue can be a potential source that influences the predictive capability of CAPS version 1.0 for longer timescales. Studies have applied bias correction techniques with different complexities for improving the performance of regional modeling system (e.g., Bruyère et al., 2014; Colette et al., 2012; Rocheta et al., 2017, 2020). Further investigation is needed to address biases inherited from GCM predictions through lateral boundaries for improving the predictive capability of CAPS version 1.0.

https://doi.org/10.5194/gmd-2021-220
Preprint. Discussion started: 12 July 2021

Geoscientific Model Development
Discussions

Code and data availability: The COAWST and CICE models are open source and can be downloaded from their developers at https://github.com/jcwarner-usgs/COAWST and https://github.com/CICE-Consortium/CICE, respectively. PDAF can be obtained from https://pdaf.awi.de/trac/wiki. CAPS v1.0 described in this paper is permanently archived at https://doi.org/10.5281/zenodo.5034971. The prediction data analyzed in this paper can be accessed from https://doi.org/10.5281/zenodo.4911415.

Author contributions: CYY and JL designed the model experiments, developed the updated CAPS model, and wrote the manuscript, CYY conducted the prediction experiments and analyzed the results. DC provided constructive feedback on the manuscript.

Competing interests: The authors declare that they have no conflict of interest.

Acknowledgements: This research is supported by the National Natural Science Foundation of China (42006188), the National Key R&D Program of China (2018YFA0605901), and the Innovation Group Project of Southern Marine Science and Engineering Guangdong Laboratory (Zhuhai) (311021008). The authors also acknowledge the National Centers for Environmental Prediction for providing CFS seasonal forecasts, the University of Hamburg for distributing the SMOS sea ice thickness data, the Alfred-Wegener-Institut, Helmholtz Zentrum für Polar- und Meeresforschung for providing the CryoSat-2 sea ice thickness data and CS2SMOS data, the Polar Science Center for distributing the PIOMAS ice thickness data, the National Snow and Ice Data Center for providing the SSMIS sea ice concentration data, the European Centre for Medium-Range Weather Forecasts for distributing the ERA5 reanalysis, and the National Oceanic and Atmospheric Administration for providing the OI sea surface temperature.

https://doi.org/10.5194/gmd-2021-220
Preprint. Discussion started: 12 July 2021



## 6. References

Bailey, D. A., Holland, M. M., DuVivier, A. K., Hunke, E. C., and Turner, A. K.: Impact of a new sea ice thermodynamic formulation in the CESM2 sea ice component. Journal of Advances in Modeling Earth Systems, 12, e2020MS002154. https://doi.org/10.1029/2020MS002154, 2020

Bitz, C. M. and Lipscomb, W. H.: An energy-conserving thermodynamic sea ice model for climate study. J. Geophys. Res.-Oceans, 104, 15669–15677, 1999.

Benjamin, S. G., Weygandt, S. S., Brown, J. M., Hu, M., Alexander, C. R., Smirnova, T. G. and Manikin, G. S.: A North American hourly assimilation and model forecast cycle: the Rapid Refresh. Monthly Weather Review, 144,1669–1694. https://doi.org/10.1175/MWR-D-15-0242.1, 2016.

Biswas, M. K., Zhang, J. A., Grell, E., Kalina, E., Newman, K., Bernardet, L., Carson, L., Frimel, J., and Grell, G.: Evaluation of the Grell–Freitas Convective Scheme in the Hurricane Weather Research and Forecasting (HWRF) Model, Weather and Forecasting, 35(3), 1017-1033, 2020.

Blanchard-Wrigglesworth, E., Bitz, C., and Holland, M.: Influence of initial conditions and climate forcing on predicting Arctic sea ice. Geophysical Research Letters, 38, L18503. https://doi.org/10.1029/2011GL048807, 2011.

Blanchard-Wrigglesworth, E., and Bushuk, M.: Robustness of Arctic sea-ice predictability in GCMs. Climate Dynamics, 52, 5555–5566, 2018.

Blanchard-Wrigglesworth, E., Cullather, R., Wang, W., Zhang, J., and Bitz, C. M.: Model forecast skill and sensitivity to initial conditions in the seasonal sea ice outlook. Geophysical Research Letters, 42, 8042–8048. https://doi.org/10.1002/2015GL065860, 2015.

Bonan, D., Bushuk, M., and Winton, M.: A spring barrier for regional predictions of summer Arctic sea ice. Geophysical Research Letter, 46, 5937–5947. https://doi.org/10.1029/2019GL082947, 2019.

https://doi.org/10.5194/gmd-2021-220
Preprint. Discussion started: 12 July 2021

Geoscientific Model Development Discussions

Briegleb, B. P. and Light, B.: A Delta-Eddington multiple scattering parameterization for solar radiation in the sea ice component of the Community Climate System Model. NCAR Tech. Note NCAR/TN-472+STR, National Center for Atmospheric Research, 2007.

Bruyère, C. L., Done, J. M., Holland, G. J., and Fredrick, S.: Bias corrections of global models for regional climate simulations of high-impact weather. Clim Dyn 43, 1847–1856 (2014). https://doi.org/10.1007/s00382-013-2011-6, 2014.

Bushuk, M., Msadek, R., Winton, M., Vecchi, G., Gudgel, R., Rosati, A., and Yang, X.: Skillful regional prediction of Arctic sea ice on seasonal timescales. Geophysical Research Letter, 44, 4953–4964. https://doi.org/10.1002/2017GL073155, 2017.

Bushuk, M., Msadek, R., Winton, M., Vecchi, G., Yang, X., Rosati, A., and Gudgel, R.: Regional Arctic sea-ice prediction: Potential versus operational seasonal forecast skill. Climate Dynamics, 52, 2721–2743, 2018.

Bushuk, M., Winton, M., Bonan, D. B., Blanchard-Wrigglesworth, E., and Delworth, T. L.: A mechanism for the Arctic sea ice spring predictability barrier. Geophysical Research Letters, 47, e2020GL088335. https://doi.org/10.1029/2020GL088335, 2020.

Cavalieri, D. J., Parkinson, C. L., Gloersen, P., and Zwally, H. J.: updated yearly. Sea Ice Concentrations from Nimbus-7 SMMR and DMSP SSM/I-SSMIS Passive Microwave Data, Version 1. Boulder, Colorado USA. NASA National Snow and Ice Data Center Distributed Active Archive Center. https://doi.org/10.5067/8GQ8LZQVL0VL, 1996.

Chen, F. and Dudhia, J.: Coupling an advanced land surface–hydrology model with the Penn State–NCAR MM5 modeling system. Part I: Model implementation and sensitivity. Mon. Wea. Rev., 129, 569–585, 2001.

Chevallier, M., Salas y Mélia, D., Voldoire, A., Déqué, M., and Garric, G.: Seasonal forecasts of the pan-Arctic sea ice extent using a GCM-based seasonal prediction system. Journal of Climate, 26(16), 6092–6104, 2013.

https://doi.org/10.5194/gmd-2021-220
Preprint. Discussion started: 12 July 2021




Colette, A., Vautard, R., and Vrac, M.: Regional climate downscaling with prior statistical correction of the global climate forcing, Geophys. Res. Lett., 39, L13707, https://doi.org/10.1029/2012GL052258, 2012.

Day, J. J., Tietsche, S., Collins, M., Goessling, H. F., Guemas, V., Guillory, A., et al.: The Arctic predictability and prediction on seasonal-to-interannual timescales (apposite) data set version 1. Geoscientific Model Development, 9, 2255–2270, 2016.

Day, J., Tietsche, S., and Hawkins, E.: Pan-Arctic and regional sea ice predictability: Initialization month dependence. Journal of Climate, 27(12), 4371–4390, 2014.

Fetterer, F., Knowles, K., Meier, W. N., Savoie, M., and Windnagel, A. K.: updated daily. Sea Ice Index, Version 3. Boulder, Colorado USA. NSIDC: National Snow and Ice Data Center. https://doi.org/10.7265/N5K072F8, 2017.

Freitas, S. R., Grell, G. A., Molod, A., Thompson, M. A., Putman, W. M., Santos e Silva, C. M. and Souza, E. P.: Assessing the Grell–Freitas convection parameterization in the NASA GEOS modeling system. J. Adv. Model. EarthSyst., 10, 1266–1289, https://doi.org/10.1029/2017MS001251, 2018.

Germe, A., Chevallier, M., y Mélia, D. S., Sanchez-Gomez, E., and Cassou, C.: Interannual predictability of Arctic sea ice in a global climate model: Regional contrasts and temporal evolution. Climate Dynamics, 43(9-10), 2519–2538, 2014.

Grell, G. A., and Freitas, S.: A scale and aerosol aware stochastic convective parameterization for weather and air quality modeling. Atmos. Chem. Phys., 14, 5233–5250, https://doi.org/10.5194/acp-14-5233-2014, 2014.

Guemas, V., Blanchard-Wrigglesworth, E., Chevallier, M., Day, J. J., Déqué, M., Doblas-Reyes, F. J., et al.: A review on Arctic sea-ice predictability and prediction on seasonal to decadal time-scales. Quarterly Journal of the Royal Meteorological Society, 142(695), 546–561, 2016.

Haidvogel, D. B., Arango, H., Budgell, W. P., Cornuelle, B. D., Curchitser, E., Di Lorenzo, E., et al.: Ocean forecasting in terrain-following coordinates: Formulation and skill

https://doi.org/10.5194/gmd-2021-220
Preprint. Discussion started: 12 July 2021

Geoscientific Model Development Discussions
Open Access

assessment of the Regional Ocean Modeling System, Journal of Computational Physics, 227, 3595–3624, 2008.

Hersbach, H., Bell, B., Berrisford, P., et al.: The ERA5 global reanalysis. Quarterly Journal of the Royal Meteorological Society, 146, 1999-2049. https://doi.org/10.1002/qj.3803, 2020.

Hunt, B. R., Kostelich, E. J., Szunyogh, I.: Efficient data assimilation for spatiotemporal chaos: A local ensemble transform Kalman filter. Physica D 230: 112–126, 2007.

Jung, T., Gordon, N.D., Bauer, P., Bromwich, D.H., Chevallier, M., Day, J.J., Dawson, J., Doblas-Reyes, F., Fairall, C., Goessling, H.F., Holland, M., Inoue, J., Iversen, T., Klebe, S., Lemke, P., Losch, M., Makshtas. A., Mills, B., Nurmi, P., Perovich, D., Reid, P., Renfrew, I.A., Smith, G., Svensson, G., Tolstykh, M., and Yang, Q.: Advancing Polar Prediction Capabilities on Daily to Seasonal Time Scales. Bulletin of the American Meteorological Society. https://doi.org/10.1175/BAMS-D-14-00246.1, 2016.

Kaleschke, L., Tian-Kunze, X., Maaß, N., Mäkynen, M., and Drusch, M.: Sea ice thickness retrieval from SMOS brightness temperatures during the Arctic freeze-up period. Geophys. Res. Lett., L05501, https://doi.org/10.1029/2012GL050916, 2012.

Kwok, R.: Arctic sea ice thickness, volume, and multiyear ice coverage: Losses and coupled variability (1958–2018). Environmental Research Letters, 13(10), 105005, 2018

Laxon, S., Giles, K. A., Ridout, A. L., Wingham, D. J., Willatt, R., Cullen, R., Kwok, R., Schweiger, A., Zhang, J., Haas, C., Hendricks, S., Krishfield, R., Kurtz, N., Farrell, S., and Davidson, M.: CryoSat-2 estimates of Arctic sea ice thickness and volume, Geophys. Res. Lett., 40, https://doi.org/10.1002/grl.50193, 2013.

Lemieux, J. F., Dupont, F., Blain, P., Roy, F., Smith, G. C., and Flato, G. M.: Improving the simulation of landfast ice by combining tensile strength and a parameterization for grounded ridges. J. Geophys. Res. Oceans, 121:7354–7368, http://dx.doi.org/10.1002/2016JC012006, 2016.

605 Liu, J., Chen, Z., Hu, Y., Zhang, Y., Ding, Y., Cheng, X., et al.: Towards reliable arctic sea ice prediction using multivariate data assimilation. Science Bulletin, 64(1), 63–72, 2019.

607 Merryfield, W., Lee, W.-S., Wang, W., Chen, M., and Kumar, A.: Multi-system seasonal predictions of Arctic sea ice. Geophysical Research Letters, 40, 1551–1556. https://doi.org/10.1002/grl.50317, 2013.

610 Maslanik, J. and Stroeve, J.: Near-Real-Time DMSP SSMIS Daily Polar Gridded Sea Ice Concentrations, Version 1. Boulder, Colorado USA. NASA National Snow and Ice Data Center Distributed Active Archive Center. https://doi.org/10.5067/U8C09DWVX9LM, 1999.

614 Msadek, R., Vecchi, G., Winton, M., and Gudgel, R.: Importance of initial conditions in seasonal predictions of Arctic sea ice extent. Geophysical Research Letters, 41, 5208–5215. https://doi.org/10.1002/2014GL060799, 2014.

617 Nakanishi, M., and Niino., H.: Development of an improved turbulence closure model for the atmospheric boundary layer. J. Meteor. Soc. Japan, 87, 895–912, https://doi.org/10.2151/jmsj.87.895, 2009.

620 Nerger, L., Danilov, S., Hiller, W., Schröter, J.: Using sea-level data to constrain a finite-element primitive-equation ocean model with a local SEIK filter, Ocean Dynamics, 56(5/6), 634-649., https://doi.org/10.1007/s10236-006-0083-0, 2006.

623 Nerger, L., and Hiller, W.: Software for Ensemble-based Data Assimilation Systems - Implementation Strategies and Scalability. Computers and Geosciences, 55, 110-118. https://doi.org/10.1016/j.cageo.2012.03.026, 2013.

626 Nerger, L., Janjić, T., Schröter, J. and Hiller, W.: A unification of ensemble square root Kalman filters. Monthly Weather Review, 140, 2335-2345. https://doi.org/10.1175/MWR-D-11-00102.1, 2012.

629 Newton, R., Pfirman, S., Schlosser, P., Tremblay, B., Murray, M. and Pomerance, R.: White Arctic vs. Blue Arctic: A case study of diverging stakeholder responses to environmental change. Earth's Future, 4: 396-405. https://doi.org/10.1002/2016EF000356, 2016.

Peterson, K., Arribas, A., Hewitt, H., Keen, A., Lea, D., and McLaren, A.: Assessing the forecast skill of Arctic sea ice extent in the GloSea4 seasonal prediction system. Climate Dynamics, 44(1-2), 147–162, 2015.

Pham, D. T.: Stochastic methods for sequential data assimilation in strongly nonlinear systems. Mon. Wea. Rev., 129, 1194–1207, 2001.

Rasch, P. J.: Conservative shape-preserving two-dimensional transport on a spherical reduced grid, Mon. Wea. Rev, 122, 1337-1350, 1994.

Reynolds, R. W., Smith, T. M., Liu, C., Chelton, D. B., Casey, K. S., and Schlax, M. G.: Daily High-Resolution-Blended Analyses for Sea Surface Temperature, Journal of Climate, 20(22), 5473-5496, 2007.

Ricker, R., Hendricks, S., Kaleschke, L., Tian-Kunze, X., King, J., and Haas, C.: A weekly Arctic sea-ice thickness data record from merged CryoSat-2 and SMOS satellite data, The Cryosphere, 11, 1607–1623, https://doi.org/10.5194/tc-11-1607-2017, 2017.

Rocheta, E., Evans, J. P., and Sharma, A.: Can Bias Correction of Regional Climate Model Lateral Boundary Conditions Improve Low-Frequency Rainfall Variability?, Journal of Climate, 30(24), 9785-9806, 2017.

Rocheta, E., Evans, J. P. and Sharma, A.: Correcting lateral boundary biases in regional climate modelling: the effect of the relaxation zone. Clim. Dyn., 55, 2511–2521. https://doi.org/10.1007/s00382-020-05393-1, 2020.

Serreze, M. C. and Meier, W. N.: The Arctic's sea ice cover: trends, variability, predictability, and comparisons to the Antarctic. Ann. N.Y. Acad. Sci., 1436: 36-53. https://doi.org/10.1111/nyas.13856, 2019.

Saha, S., Moorthi, S., Wu, X., et al.: The NCEP climate forecast system version 2. J. Clim. 27:2185–2208, 2014.

Shchepetkin, A.F., McWilliams, J. C.: Quasi-monotone advection schemes based on explicit locally adaptive dissipation. Mon. Weather Rev. 126 (6), 1541–1580, 1998.

658 Shchepetkin, A. F., and McWilliams, J. C.: The Regional Ocean Modeling System: A split-explicit, free-surface, topography following coordinates ocean model, Ocean Modelling, 9, 347-404, 2005.

661 Sigmond, M., Fyfe, J., Flato, G., Kharin, V., and Merryfield, W.: Seasonal forecast skill of Arctic sea ice area in a dynamical forecast system. Geophysical Research Letters, 40, 529–534. https://doi.org/10.1002/grl.50129, 2013.

664 Skamarock, W. C., Klemp, J. B., Dudhia, J., Gill, D. O., Barker, D. M., Wang, W. and Powers, J. G.: A Description of the Advanced Research WRF Version 2. NCAR Technical Note, NCAR/TN-468+STR, 2005.

667 Smolarkiewicz, P. K.: Multidimensional positive definite advection transport algorithm: An overview. Int. J. Numer. Methods Fluids, 50, 1123–1144, 2006.

669 Song, Y. and Haidvogel, D. B.: A semi-implicit ocean circulation model using a generalized topography-following coordinate system. J. Comp. Phys., 115(1), 228-244, 1994.

671 Stroeve, J., Blanchard-Wrigglesworth, E., Guemas, V., Howell, S., Massonnet, F., and Tietsche, S.: Improving predictions of Arctic sea ice extent, Eos, 96, https://doi.org/10.1029/2015EO031431, 2015.

674 Stroeve, J., Hamilton, L. C., Bitz, C. M., and Blanchard-Wrigglesworth, E.: Predicting September sea ice: Ensemble skill of the SEARCH Sea Ice Outlook 2008 – 2013, Geophys. Res. Lett., 41, 2411-2418, https://doi.org/10.1002/2014GL059388, 2014.

677 Tian-Kunze, X., Kaleschke, L., Maaß, N., Mäkynen, M., Serra, N., Drusch, M., and Krumpen, T.: SMOS-derived thin sea ice thickness: Algorithm baseline, product specifications and initial verification. Cryosphere, 8, 997-1018, https://doi.org/10.5194/tc-8-997-2014, 2014.

681 Tietsche, S., Day, J., Guemas, V., Hurlin, W., Keeley, S., Matei, D., et al.: Seasonal to interannual Arctic sea ice predictability in current global climate models. Geophysical Research Letters, 41, 1035–1043. https://doi.org/10.1002/2013GL058755, 2014.

https://doi.org/10.5194/gmd-2021-220
Preprint. Discussion started: 12 July 2021



Turner, A. K., and Hunke, E. C.: Impacts of a mushy-layer thermodynamic approach in global sea-ice simulations using the CICE sea-ice model, J. Geophys. Res. Oceans, 120, 1253-1275, doi:10.1002/2014JC010358, 2015.

Turner, A. K., Hunke, E. C., and Bitz, C. M.: Two modes of sea-ice gravity drainage: A parameterization for large-scale modeling, J. Geophys. Res., 118, 2279–2294, doi:10.1002/jgrc.20171, 2013.

Van den Dool, H.: Empirical Methods in Short-Term Climate Prediction, Oxford Univ. Press, Oxford, U. K., 2006.

Wang, W., Chen, M., and Kumar, A.: Seasonal prediction of Arctic sea ice extent from a coupled dynamical forecast system. Monthly Weather Review, 141(4), 1375–1394, 2013.

Warner, J. C., Armstrong, B., He, R., and Zambon, J.: Development of a coupled ocean–atmosphere–wave–sediment transport (COAWST) modeling system. Ocean Modell. 35, 230–244, 2010.

Wu, W., Lynch, A. H., and Rivers, A.: Estimating the Uncertainty in a Regional Climate Model Related to Initial and Lateral Boundary Conditions, Journal of Climate, 18(7), 917-933, 2005.

Yang, C.-Y., Liu, J., and Xu, S.: Seasonal Arctic sea ice prediction using a newly developed fully coupled regional model with the assimilation of satellite sea ice observations. Journal of Advances in Modeling Earth Systems, 12, e2019MS001938. https://doi.org/10.1029/2019MS001938, 2020.

Zampieri, L., Goessling, H. F., and Jung, T.: Bright prospects for Arctic sea ice prediction on subseasonal time scales. Geophysical Research Letters, 45, 9731– 9738. https://doi.org/10.1029/2018GL079394, 2018.

Zhang, J. and Rothrock, D.: Modeling global sea ice with a thickness and enthalpy distribution model in generalized curvilinear coordinates. Mon. Wea. Rev., 131, 845–861, 2003.

https://doi.org/10.5194/gmd-2021-220
Preprint. Discussion started: 12 July 2021

Geoscientific Model Development
Discussions

## 7. Tables

Table 1 Difference in versions for the model components between the original and updated CAPS

| | Yang et al. (2020) | This paper |
|---|---|---|
| COAWST | 3.1 | 3.5 |
| WRF | 3.6.1 | 4.1.2 |
| ROMS | 3.7 revision 748 | 3.8 revision 981 |
| CICE | 5.1.2 | 6.0.0 |

https://doi.org/10.5194/gmd-2021-220
Preprint. Discussion started: 12 July 2021

Geoscientific Model Development Discussions
Open Access EGU

715 Table 2 The summary of physic parameterizations used in the Y21_CRTL experiment

| | |
|---|---|
| WRF physics | |
| Cumulus parameterization | Grell-Freitas (Freitas et al. 2018; improved from Y20) |
| Microphysics parameterization | Morrison 2-moment (Morrison et al. 2009; same as Y20) |
| Longwave radiation parameterization | CAM spectral band scheme (Collins et al. 2004; same as Y20) |
| Shortwave radiation parameterization | CAM spectral band scheme (Collins et al. 2004; same as Y20) |
| Boundary layer physics | MYNN2 (Nakanishi and Niino, 2006; improved from Y20) |
| Land surface physics | Unified Noah LSM (Chen and Dudhia, 2001; improved from Y20) |
| | |
| ROMS physics | |
| Tracer advection scheme | MPDATA (Smolarkiewicz, 2006; same as Y20) |
| Tracer vertical mixing scheme | GLS (Umlauf and Burchard, 2003; same as Y20) |

https://doi.org/10.5194/gmd-2021-220
Preprint. Discussion started: 12 July 2021



| | |
|---|---|
| Bottom drag scheme | Quadratic bottom friction (QDRAG; (same as Y20) |
| | |
| CICE physics | |
| Ice dynamics | EVP (Hunke and Dukowicz, 1997; improved from Y20) |
| Ice thermodynamics | Bitz and Lipscomb (1999; same as Y20) |
| Shortwave albedo | Delta-Eddington (Briegleb and Light, 2007; same as Y20) |

https://doi.org/10.5194/gmd-2021-220
Preprint. Discussion started: 12 July 2021

Geoscientific Model Development Discussions
Open Access

Table 3 The summary of the prediction experiments and details of experiment designs. Note: All experiments use the CFS operational forecasts as initial and boundary conditions; VT: vertical transformation function; VS: vertical stretching function; SH94: stretching function of Song and Haidvogel (1994); S10: stretching function of Shchepetkin (2010).

| Experiment | Physics | Assimilation | ROMS vertical coordinate | Simulation period |
|---|---|---|---|---|
| Y20 | Physics (old version) listed in Table 2 | 2 localization radii<br>SSMIS SIC<br>Simply-merged CryoSat-2/SMOS SIT | VT 1<br>VS SH94<br>$h_c$ 10m | 2018.07.01-2018.10.01 |
| Y20_MOD | Physics (old version) listed in Table 2 | 6 localization radii<br>SSMIS SIC<br>Simply-merged CryoSat-2/SMOS SIT | VT 1<br>VS SH94<br>$h_c$ 10m | 2018.07.01-2018.10.01 |
| Y21_CTRL | Physics (new version) listed in Table 2 | 6 localization radii<br>SSMIS SIC<br>Simply-merged CryoSat-2/SMOS SIT | VT 1<br>VS SH94<br>$h_c$ 10m | 2018.07.01-2018.10.01 |
| Y21_VT | Physics (new version) | 6 localization radii | VT 2 | 2018.07.01- |

https://doi.org/10.5194/gmd-2021-220
Preprint. Discussion started: 12 July 2021

Geoscientific Model Development Discussions
Open Access
EGU

| | | | | |
|---|---|---|---|---|
| | listed in Table 2 | SSMIS SIC<br>Simply-merged CryoSat-2/SMOS SIT | VS S10<br>$h_c$ 300m | 2018.10.01 |
| Y21_RP | Advection: U3H/C4V<br>Bottom drag: LOGDRAG | 6 localization radii<br>SSMIS SIC<br>Simply-merged CryoSat-2/SMOS SIT | VT 2<br>VS S10<br>$h_c$ 300m | 2018.07.01-2018.10.01 |
| Y21_MUSHY | Same physics as Y21_RP<br>CICE: Mushy layer thermodynamics | 6 localization radii<br>SSMIS SIC<br>Simply-merged CryoSat-2/SMOS SIT | VT 2<br>VS S10<br>$h_c$ 300m | 2018.07.01-2018.10.01 |
| Y21_ SIT | Same physics as Y21_RP | 6 localization radii<br>SSMIS SIC<br>OI-merged CryoSat-2/SMOS SIT | VT 2<br>VS S10<br>$h_c$ 300m | 2018.07.01-2018.10.01 |
| Y21_EXT-7 | Same physics as Y21_RP | 6 localization radii<br>SSMIS SIC<br>OI-merged CryoSat-2/SMOS SIT | VT 2<br>VS S10<br>$h_c$ 300m | 2018.07.01-2019.01.31 |
| Y21_MAR-7 | Same physics as | 6 localization radii | VT 2 | 2018.03.01- |

https://doi.org/10.5194/gmd-2021-220
Preprint. Discussion started: 12 July 2021

Geoscientific Model Development Discussions

| | | | | |
|---|---|---|---|---|
| | Y21_RP | SSMIS SIC<br>OI-merged CryoSat-2/SMOS SIT | VS S10<br>$h_c$ 300m | 2018.09.30 |

https://doi.org/10.5194/gmd-2021-220
Preprint. Discussion started: 12 July 2021


Geoscientific Model Development Discussions
Open Access
EGU

724 **8. Figures**

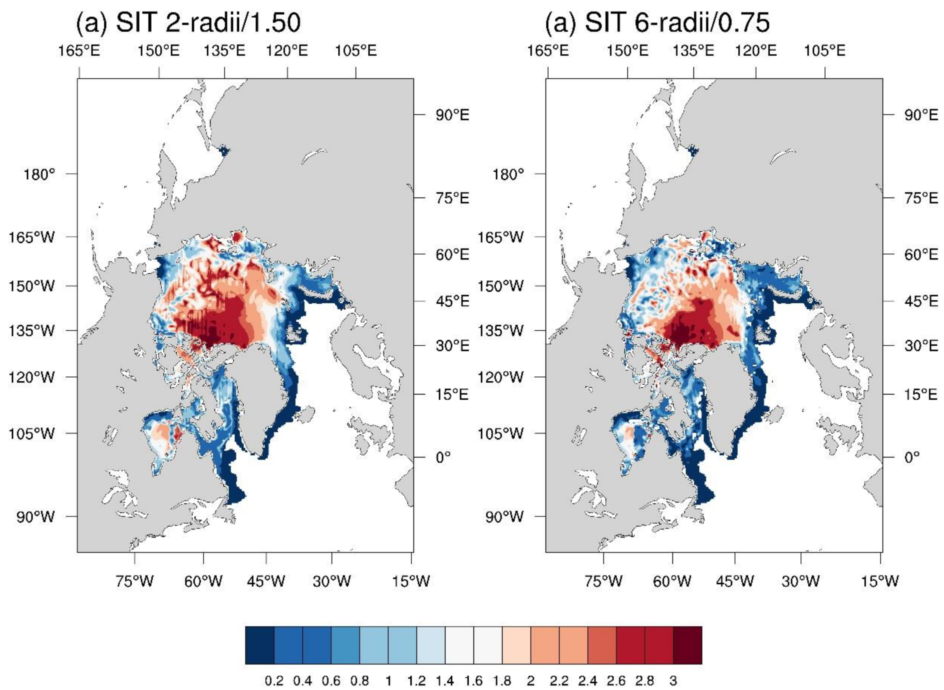


725

726 Figure 1 The initial sea ice thickness after data assimilation with (a) 2 localization radii/1.5m
727 ice thickness uncertainty, and (b) 6 localization radii/0.75m ice thickness uncertainty.

728

https://doi.org/10.5194/gmd-2021-220
Preprint. Discussion started: 12 July 2021


Geoscientific Model Development
Discussions
Open Access
EGU

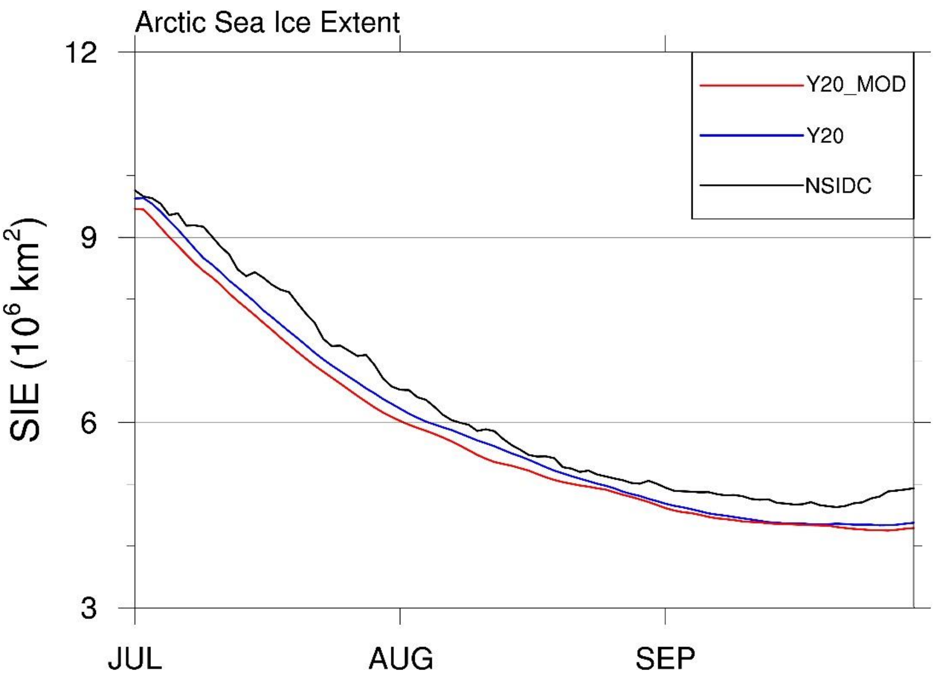


Figure 2 Time-series of Arctic sea ice extent for the observations (black line) and the ensemble-mean of Y20 (blue line) and Y20_MOD (red line).

https://doi.org/10.5194/gmd-2021-220
Preprint. Discussion started: 12 July 2021




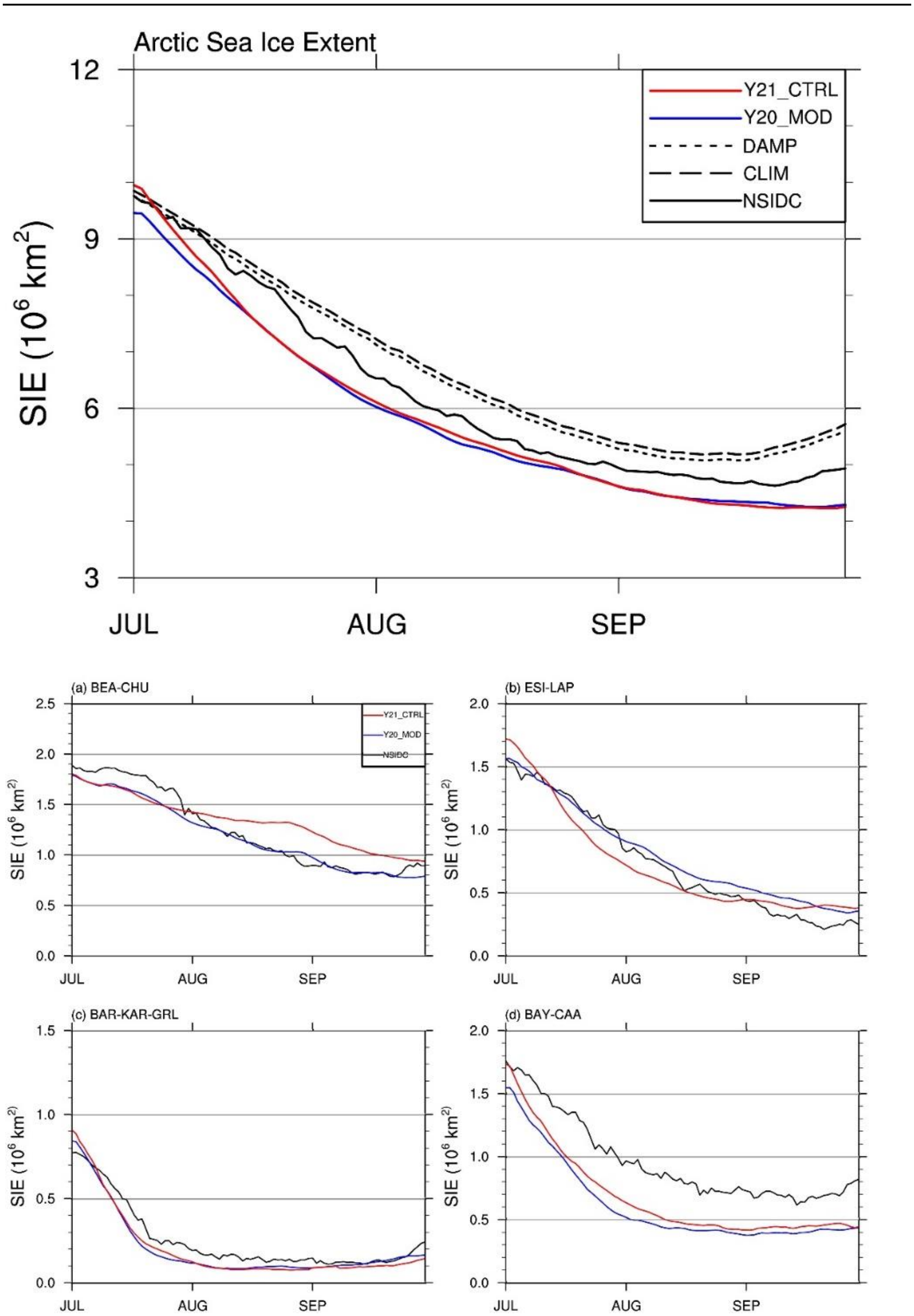


733

https://doi.org/10.5194/gmd-2021-220
Preprint. Discussion started: 12 July 2021

Geoscientific Model Development
Discussions

Figure 3 Top panel: Time-series of Arctic sea ice extent for the observations (black line) and the ensemble-mean of Y20_MOD (blue line) and Y21_CTRL (red line). Dashed and dotted lines are the climatology and the damped anomaly persistence predictions. Bottom panel: Time-series of the observed (black line) and the ensemble-mean of regional sea ice extents for Y20_MOD (blue line) and Y21_CTRL (red line). (a) Beaufort-Chukchi Seas, (b) East Siberian-Laptev Seas, (c) Barents-Kara-Greenland Seas, and (d) Baffin Bay-Canadian Archipelago.

https://doi.org/10.5194/gmd-2021-220
Preprint. Discussion started: 12 July 2021



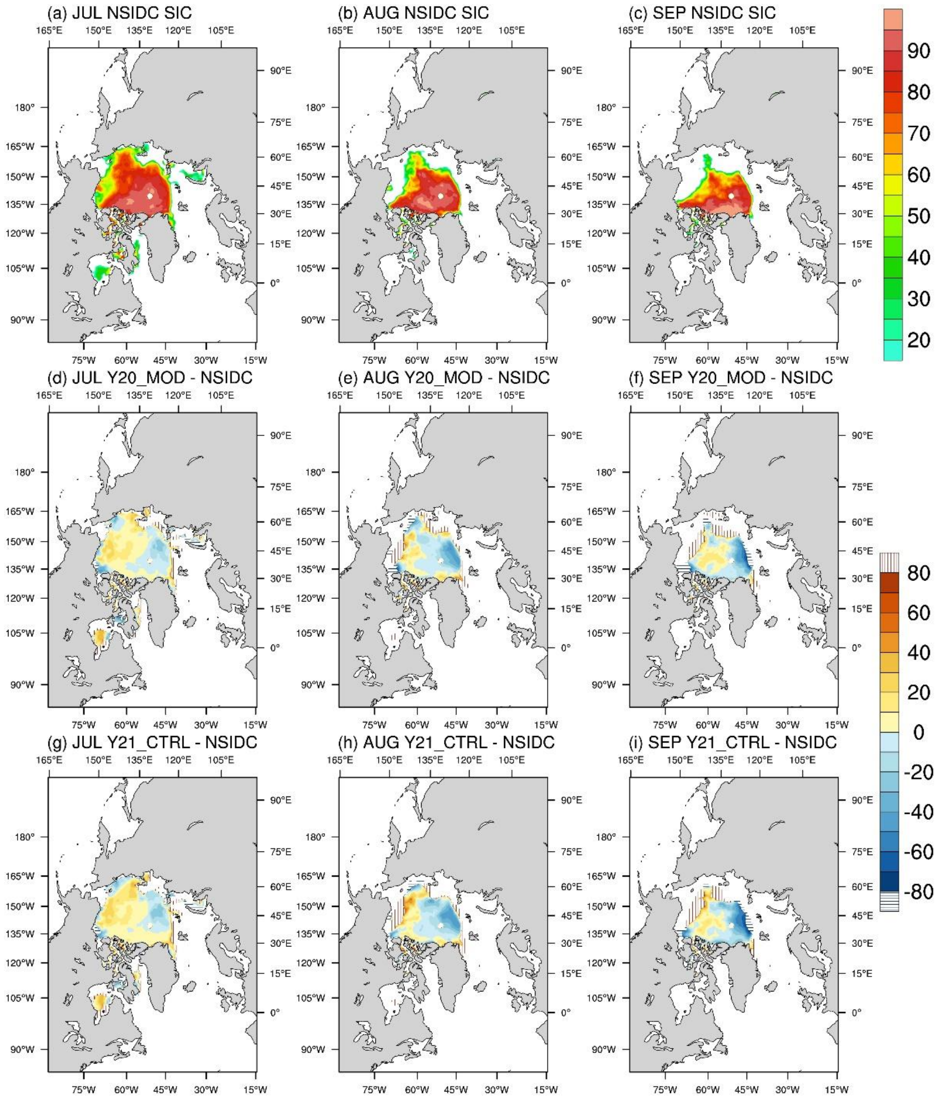


Figure 4 Monthly mean of sea ice concentration for (a) July, (b) August, (c) September of the NSIDC observations, and the difference between the predictions and the observations for (d) July, (e) August, (f) September of Y20_MOD, (g) July, (h) August, and (i) September of Y21_CTRL. Vertical/horizontal-line areas represent the difference of ice edge location (15% concentration).

https://doi.org/10.5194/gmd-2021-220
Preprint. Discussion started: 12 July 2021

Geoscientific Model Development
Discussions

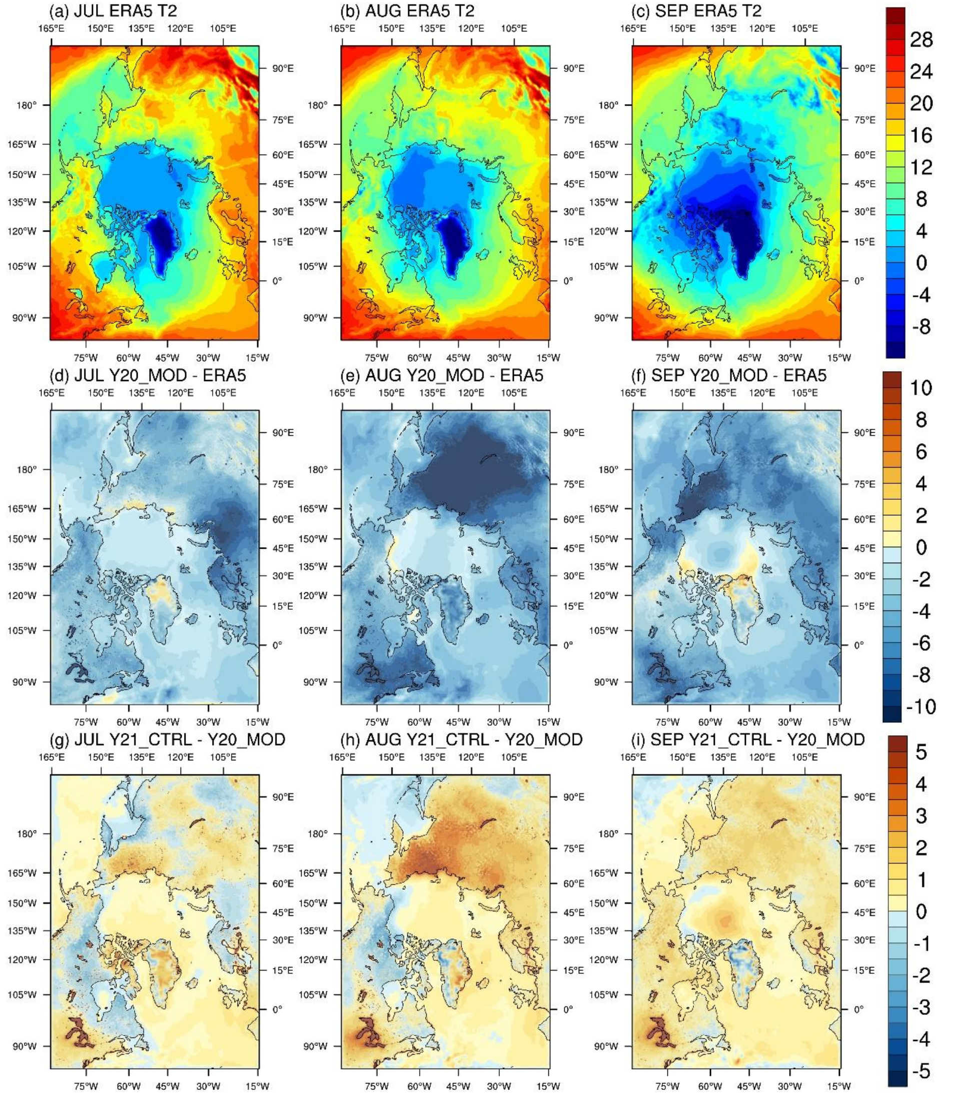


Figure 5 ERA5 monthly mean of near-surface air temperature for (a) July, (b) August, and (c) September, the difference between Y20_MOD and ERA5 for (d) July, (e) August, (f) September, and the difference between Y21_CTRL and Y20_MOD for (g) July, (h) August, and (i) September.

https://doi.org/10.5194/gmd-2021-220
Preprint. Discussion started: 12 July 2021


Geoscientific Model Development
Discussions

753 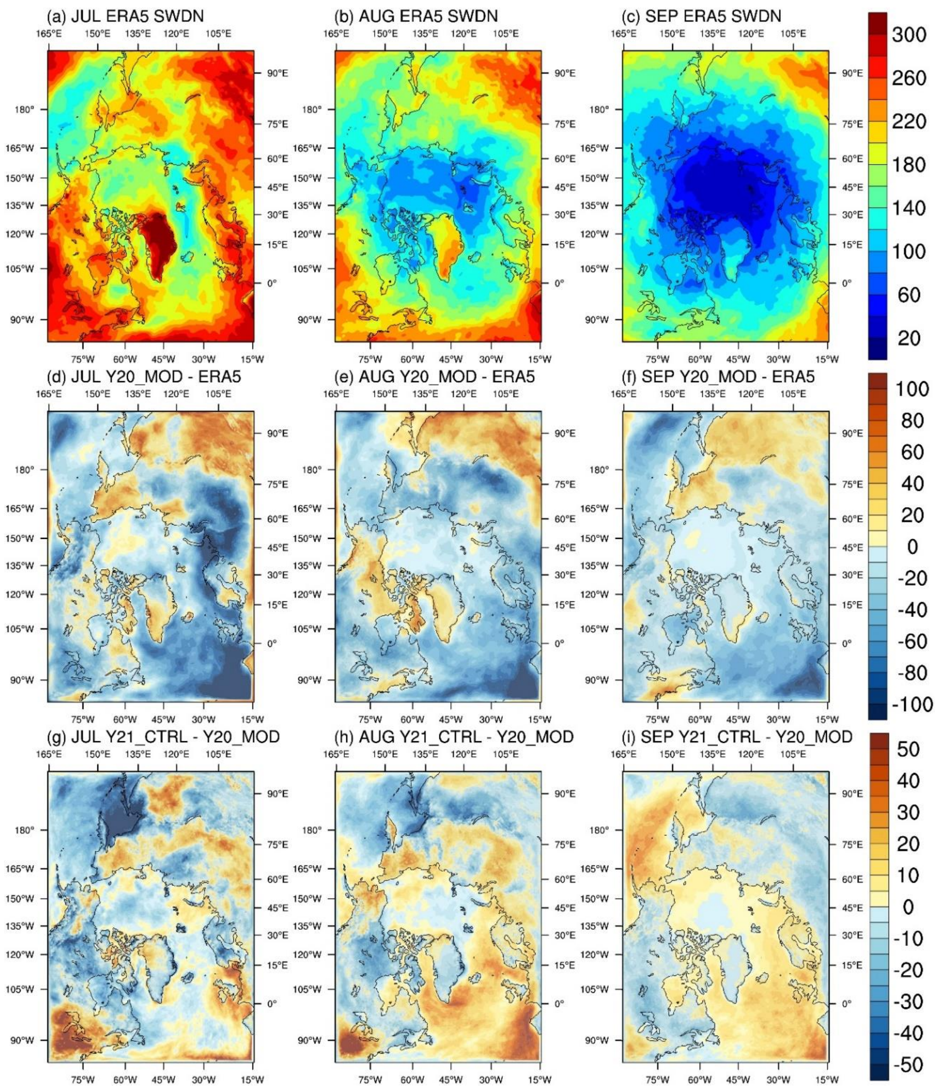


754 Figure 6 Same as Figure 5, but for downward shortwave radiation at the surface.

755

https://doi.org/10.5194/gmd-2021-220
Preprint. Discussion started: 12 July 2021



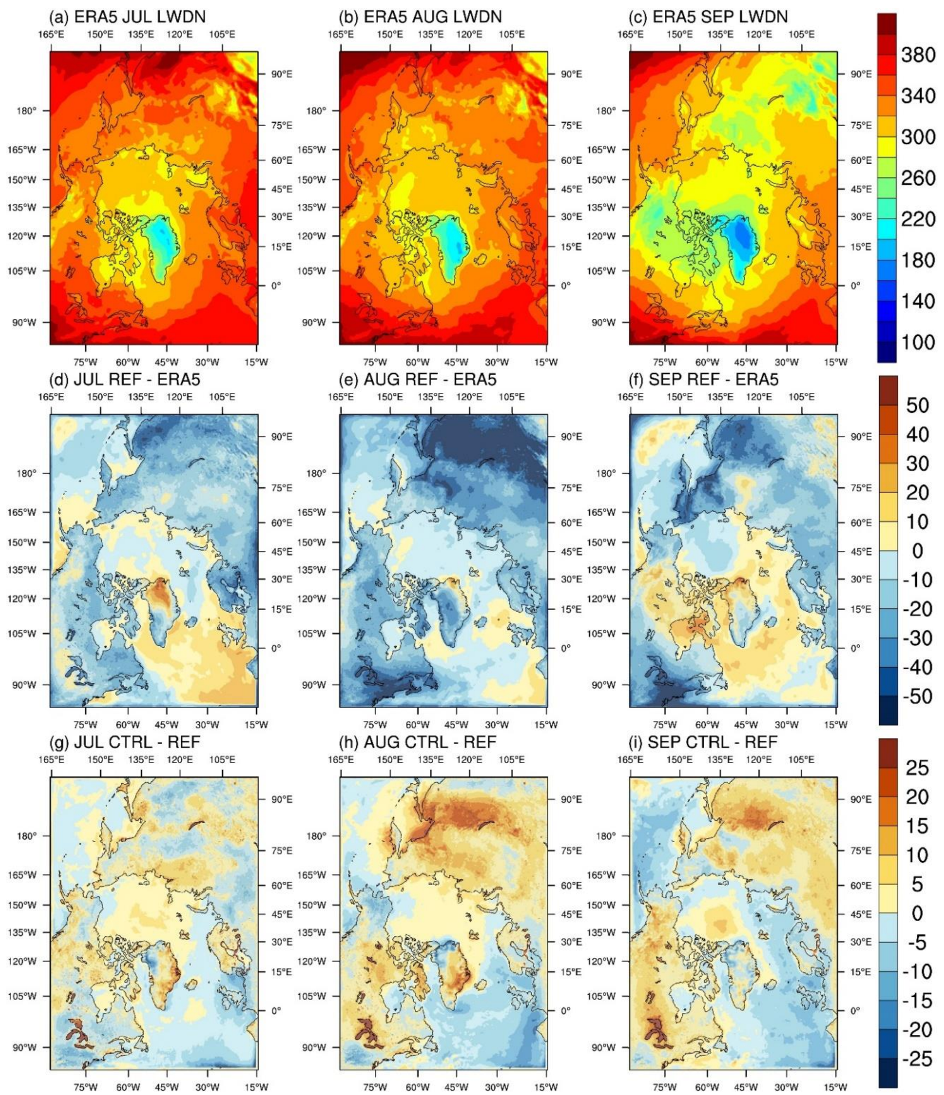


Figure 7 Same as Figure 6, but for downward thermal radiation at the surface.

https://doi.org/10.5194/gmd-2021-220
Preprint. Discussion started: 12 July 2021



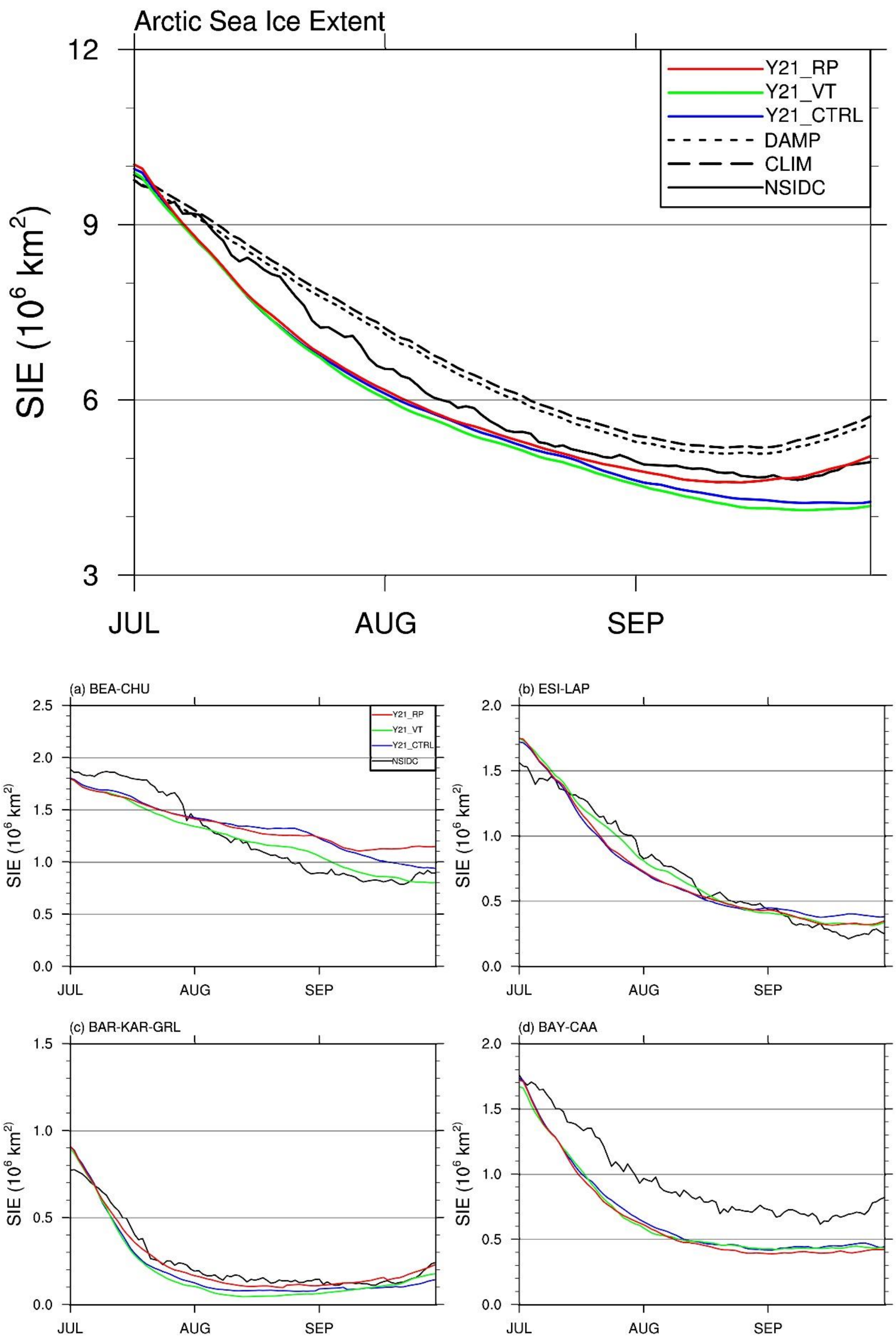

https://doi.org/10.5194/gmd-2021-220
Preprint. Discussion started: 12 July 2021


Figure 8 Same as Figure 3, but for Y21_CTRL (blue line), Y21_VT (green line), and Y21_RP (red line).

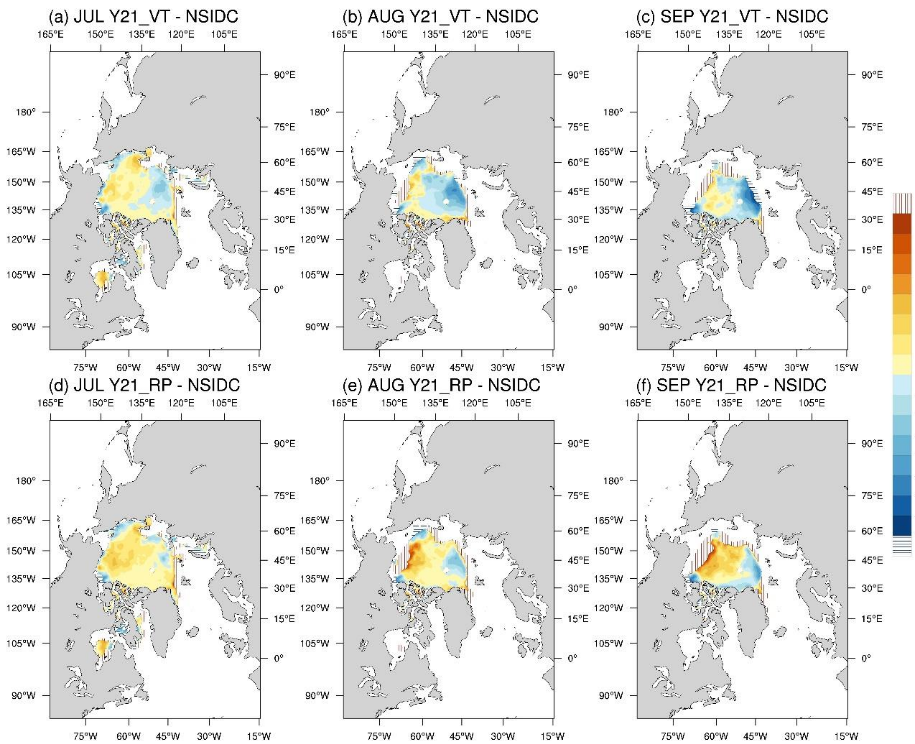


Figure 9 Monthly mean of sea ice concentration difference between the predictions and the observations for (a) July, (b) August, (c) September of Y21_VT, (d) July, (e) August, and (f) September of Y21_RP. Vertical/horizontal-line areas represent the difference of ice edge location (15% concentration).

https://doi.org/10.5194/gmd-2021-220
Preprint. Discussion started: 12 July 2021




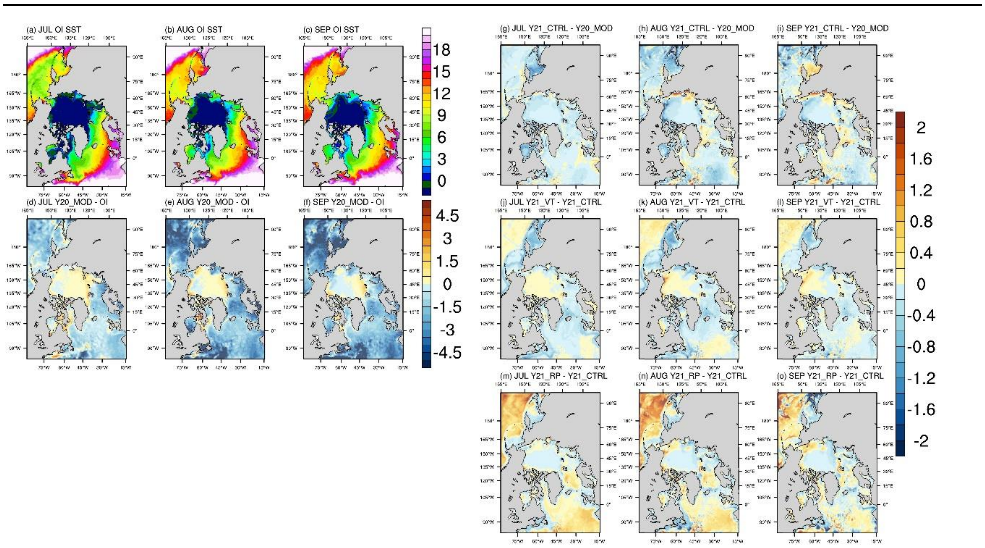


Figure 10 Left panel: Monthly mean of sea surface temperature for (a) July, (b) August, (c) September of the OI SST, and the difference between the predictions and the observations for (d) July, (e) August, (f) September of Y20_MOD. Right panel: Monthly mean of sea surface temperature difference between Y21_CTRL and Y20_MOD for (g) July, (h) August, (i) September, and the difference between Y21_VT/Y21_RP and Y21_CTRL for (j) July, (k) August, (l) September of Y21_VT, (m) July, (n) August, and (o) September of Y21_RP.

https://doi.org/10.5194/gmd-2021-220
Preprint. Discussion started: 12 July 2021

Geoscientific Model Development
Discussions

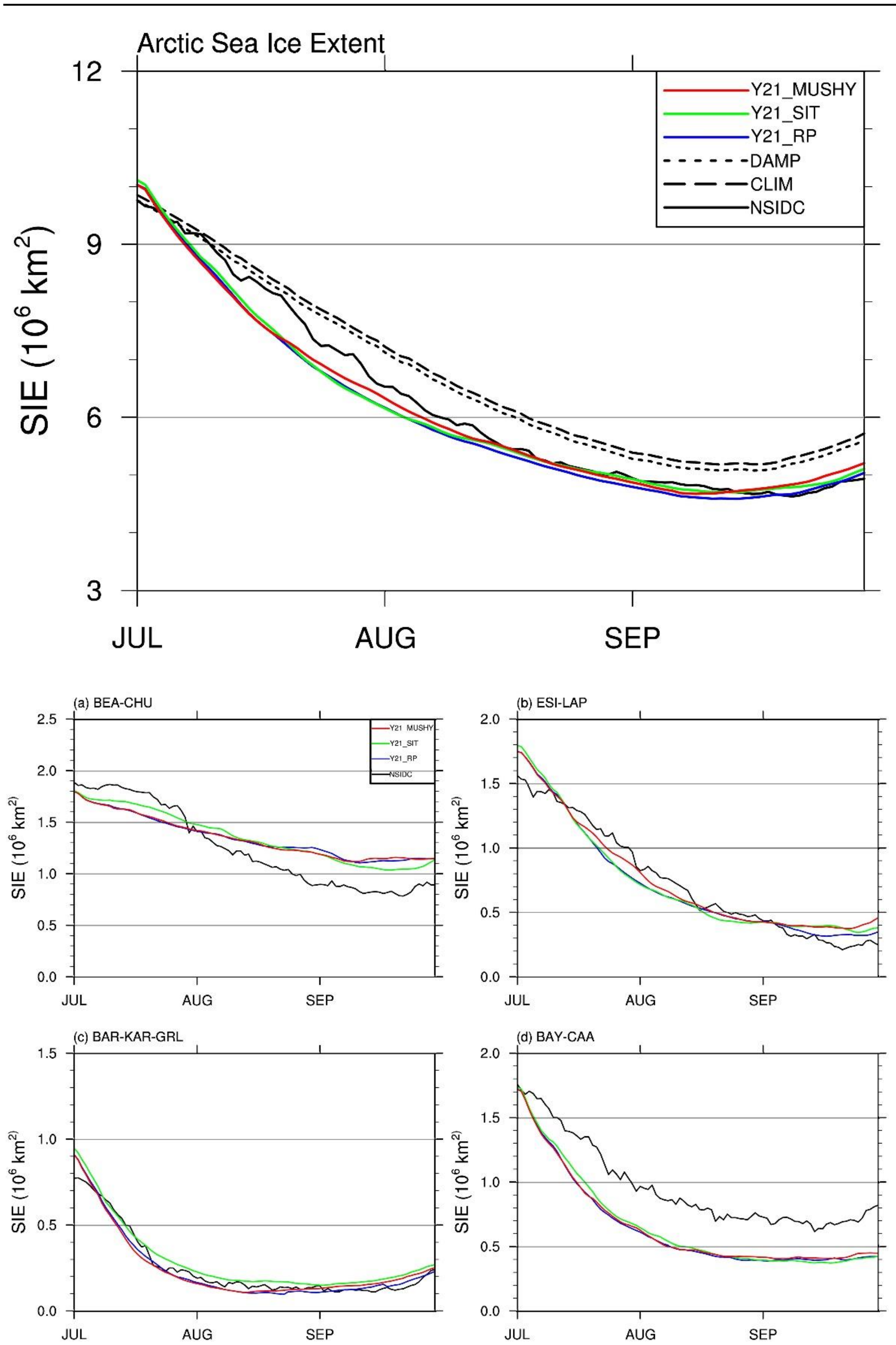


776

777 Figure 11 Same as Figure 3, but for Y21_RP, Y21_MUSHY, and Y21_SIT.

https://doi.org/10.5194/gmd-2021-220
Preprint. Discussion started: 12 July 2021



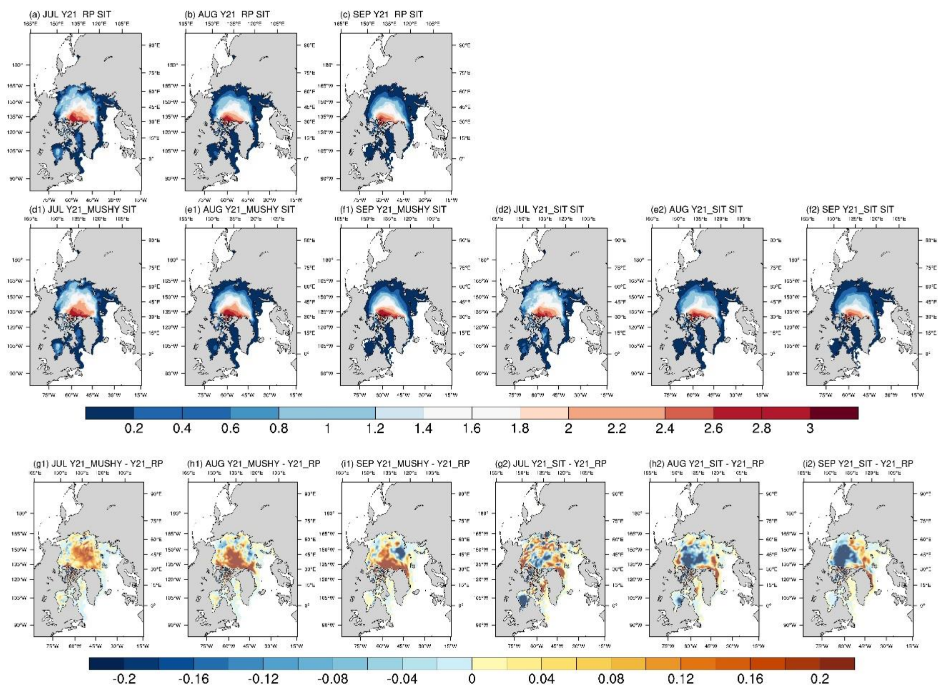


Figure 12 Monthly mean of sea ice thickness for (a) July, (b) August, and (c) September of Y21_RP, ($d_1$) July, ($e_1$) August, ($f_1$) September of Y21_MUSHY, ($d_2$) July, ($e_2$) August, ($f_2$) September of Y21_SIT, the difference between Y21_MUSHY and Y21_RP for ($g_1$) July, ($h_1$) August, and ($i_1$) September, and the difference between Y21_SIT and Y21_RP for ($g_2$) July, ($h_2$) August, and ($i_2$) September.

https://doi.org/10.5194/gmd-2021-220
Preprint. Discussion started: 12 July 2021

Geoscientific Model Development Discussions

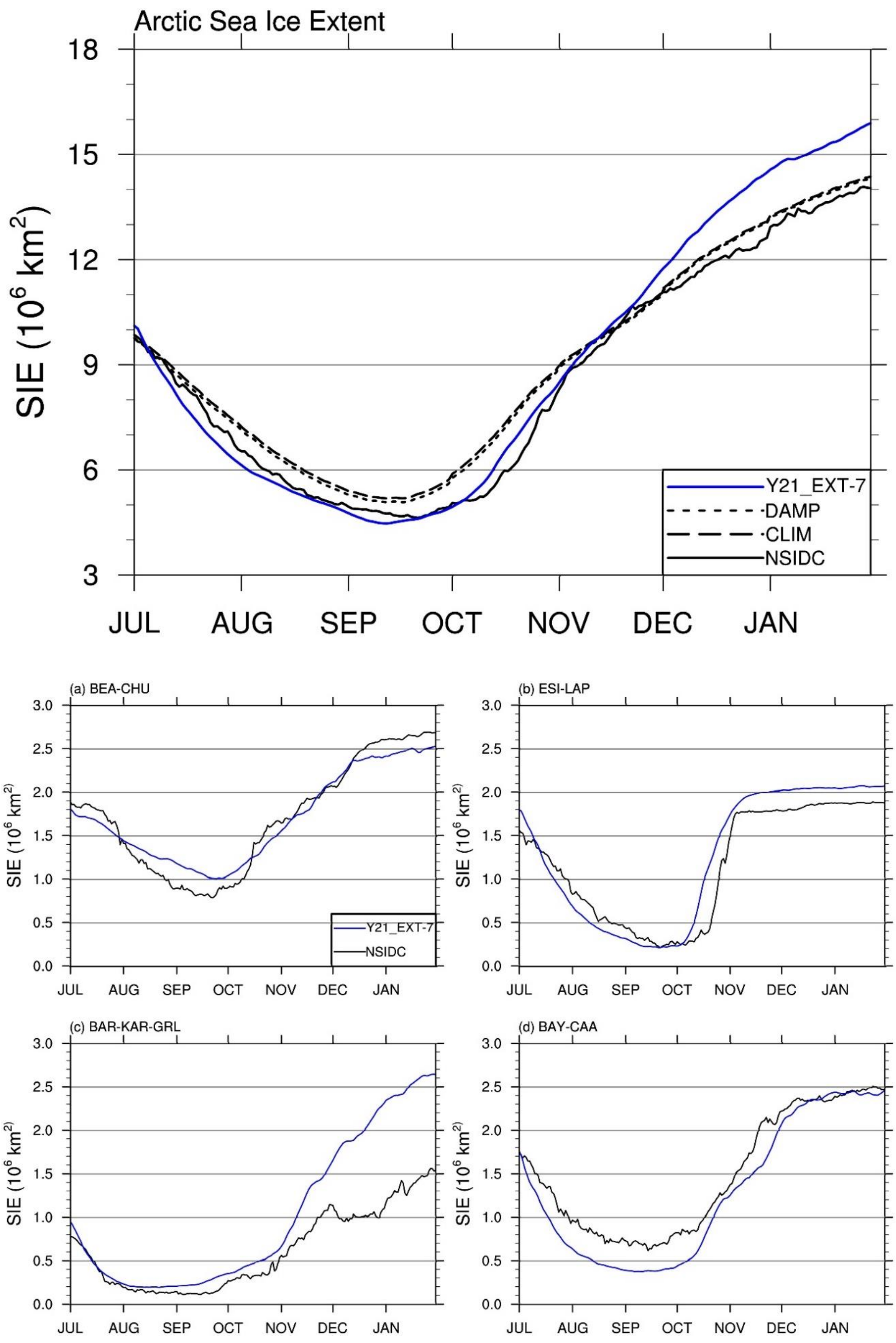


786

787 Figure 13 Same as Figure 3, but for Y21_EXT-7.

https://doi.org/10.5194/gmd-2021-220
Preprint. Discussion started: 12 July 2021


Geoscientific Model Development
Discussions

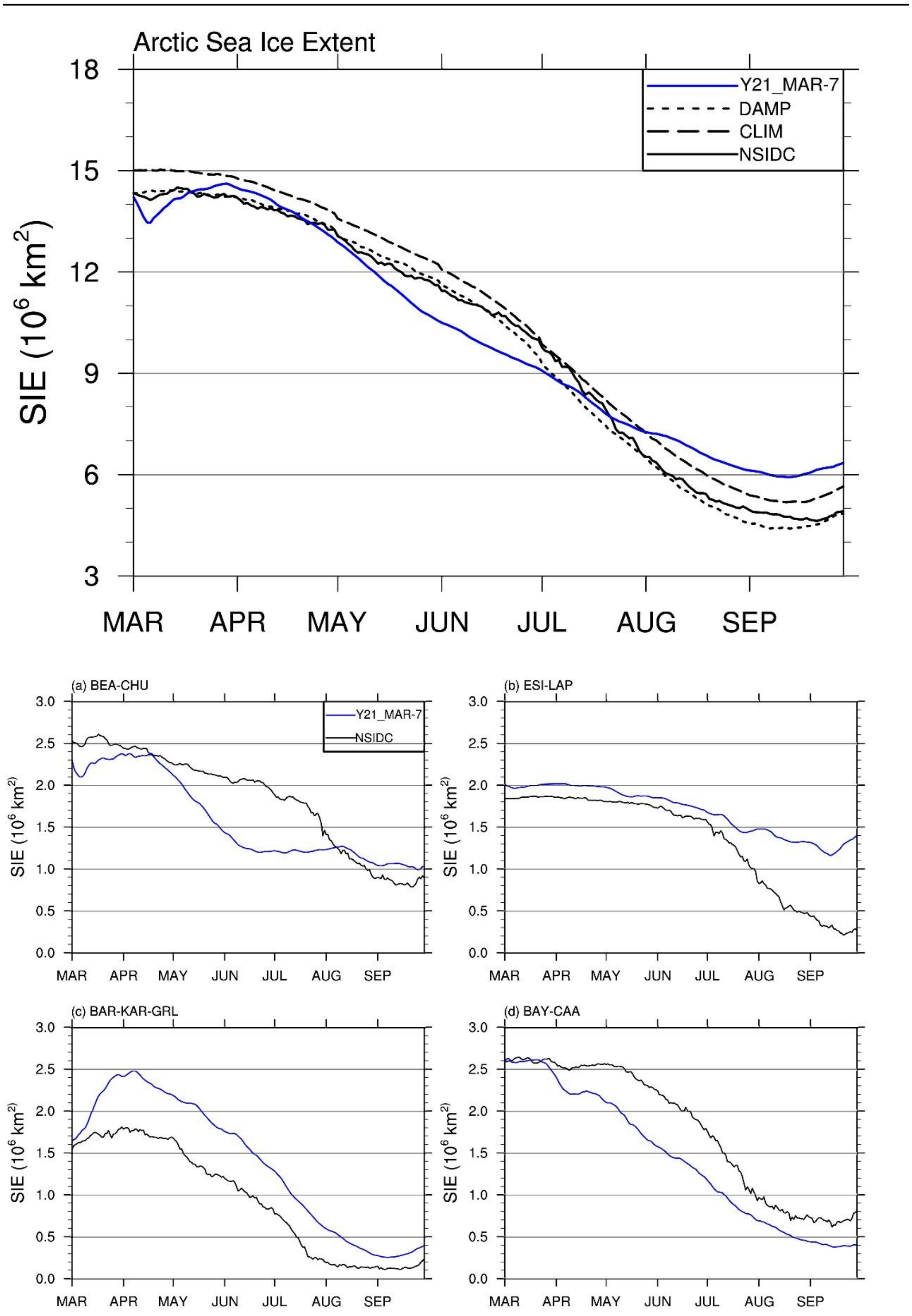


789

790 Figure 14 Same as Figure 3, bur for Y21_MAR-7.